SUMO paralogue–specific functions revealed through systematic analysis of human knockout cell lines and gene expression data

Danielle Bouchard, Wei Wang, Wei-Chih Yang, Shuying He, Anthony Garcia, and Michael J. Matunis*
Department of Biochemistry and Molecular Biology, Johns Hopkins University Bloomberg School of Public Health, Baltimore, MD 21205

ABSTRACT The small ubiquitin-related modifiers (SUMOs) regulate nearly every aspect of cellular function, from gene expression in the nucleus to ion transport at the plasma membrane. In humans, the SUMO pathway has five SUMO paralogues with sequence homologies that range from 45% to 97%. SUMO1 and SUMO2 are the most distantly related paralogues and also the best studied. To what extent SUMO1, SUMO2, and the other paralogues impart unique and nonredundant effects on cellular functions, however, has not been systematically examined and is therefore not fully understood. For instance, knockout studies in mice have revealed conflicting requirements for the paralogues during development and studies in cell culture have relied largely on transient paralogue overexpression or knockdown. To address the existing gap in understanding, we first analyzed SUMO paralogue gene expression levels in normal human tissues and found unique patterns of *SUMO1–3* expression across 30 tissue types, suggesting paralogue-specific functions in adult human tissues. To systematically identify and characterize unique and nonredundant functions of the SUMO paralogues in human cells, we next used CRISPR-Cas9 to knock out SUMO1 and SUMO2 expression in osteosarcoma (U2OS) cells. Analysis of these knockout cell lines revealed essential functions for SUMO1 and SUMO2 in regulating cellular morphology, promyelocytic leukemia (PML) nuclear body structure, responses to proteotoxic and genotoxic stress, and control of gene expression. Collectively, our findings reveal nonredundant regulatory roles for SUMO1 and SUMO2 in controlling essential cellular processes and provide a basis for more precise SUMO-targeting therapies.

INTRODUCTION

Small ubiquitin-related modifiers (SUMOs) function as posttranslational protein modifications that regulate a broad range of cellular

functions including chromosome segregation, DNA damage repair, gene expression, cellular stress responses, mitochondrial fission, and ion channel activity (Wasik and Filipek, 2014; Eifler and Vertegaal, 2015; Zhao, 2018; Chang and Yeh, 2020). At the molecular level, SUMO shares only 18% sequence homology with ubiquitin; however, many similarities exist between the SUMO and ubiquitin protein modification pathways. Like ubiquitin, SUMOs are conjugated to other proteins through an enzyme cascade involving an E1 activating enzyme, an E2 conjugating enzyme, and E3 ligases (Cappadocia and Lima, 2018). Sumoylation of most proteins is also highly dynamic and reversible through the action of SUMO-specific isopeptidases (Hickey *et al.*, 2012). Similar to ubiquitin, SUMO is also recognized as a molecular signal that promotes protein–protein interactions between modified substrates and downstream effector proteins. Given their divergent sequences, however, SUMO and ubiquitin mediate interactions with distinct effectors (Hay, 2013). In

addition, the SUMO and ubiquitin pathways diverge at the level of the modifying proteins themselves. In contrast to a single ubiquitin protein, most multicellular organisms, including plants, vertebrates, and basal insects, express multiple SUMO paralogues (Citro and Chiocca, 2013; Urena *et al.*, 2016; Augustine and Vierstra, 2018). Despite their expansion and conservation across species, the functional significance of SUMO paralogues and why they evolved remains an important question for the field.

Humans express five SUMO paralogues, SUMO1–5, that share 45–97% sequence identity. Of the paralogues, SUMO1–3 are the most widely studied. Following processing, SUMO2 and SUMO3 share ~97% peptide sequence identity and are thus often referred to as SUMO2/3. In contrast, SUMO1 shares only ~45% sequence identity with SUMO2/3, suggesting that these paralogues may have unique properties that allow them to be recognized as distinct signals. Consistent with this, a number of studies have revealed unique SUMO1 and SUMO2/3 subcellular localization patterns and dynamics (Ayaydin and Dasso, 2004; Zhang *et al.*, 2008b). Other studies have identified proteins that interact preferentially with SUMO1 or SUMO2/3 through variant SUMO-interacting motifs (SIMs) (Hecker *et al.*, 2006; Rosendorff *et al.*, 2006; Ghisletti *et al.*, 2007; Meulmeester *et al.*, 2008; Zhu *et al.*, 2008; Ouyang *et al.*, 2009; Chang *et al.*, 2011, 2013; Namanja *et al.*, 2012). In addition, SUMO2/3 contains an internal consensus site lysine at position 11 that allows for efficient assembly of SUMO2/3 polymeric chains (Tatham *et al.*, 2001). Among other possible functions, SUMO2/3 polymeric chains are recognized by SUMO-targeted ubiquitin ligases (STUbLs) and can thereby target proteins for degradation through the ubiquitin-proteasome system (Sriramachandran and Dohmen, 2014; Jansen and Vertegaal, 2021). SUMO1 lacks a consensus site lysine and thus has reduced potential to form polymeric chains. The ability to associate differentially with SIM-containing proteins and to form polymeric chains may be defining features that distinguish SUMO1 from SUMO2/3 function, although the contributions of these features to unique functions remain to be fully tested. SUMO4 and SUMO5 are the least well understood, although limited studies suggest that both paralogues have restricted expression to specific tissues (Wang and She, 2008; Liang *et al.*, 2016).

At the organismal level, genetic knockout studies in vertebrates have provided conflicting results on the essential functions of individual SUMO paralogues. Whereas SUMO1 expression is uniquely required for development in *Xenopus laevis*, each of SUMO1, SUMO2, and SUMO3 is dispensable for development in zebrafish (Yukita *et al.*, 2007; Yuan *et al.*, 2010). In mice, SUMO2 is essential for embryonic development, but SUMO3 is not (Wang *et al.*, 2014). Moreover, functions for SUMO1 in mice are less clear, as it has been reported to be both critical and dispensable for embryonic development (Alkuraya *et al.*, 2006; Evdokimov *et al.*, 2008; Zhang et al., 2008a). Studies focused on the roles of the paralogues in development are further complicated by the fact that they do not reveal possible essential functions postdevelopment. In this regard, otherwise normal, adult SUMO1 knockout mice have dramatically different responses to a high-fat diet (Mikkonen *et al.*, 2013). Unique roles for the SUMO paralogue postembryonic development are also supported by studies at the tissue level, including in the placenta, intestine, eye, and brain. In each of these tissues, SUMO1 and SUMO2/3 exhibit remarkably different expression and localization patterns (Gong and Li, 2010; Hasegawa *et al.*, 2014; Baczyk *et al.*, 2018; Karhausen *et al.*, 2018).

Numerous studies in cell culture have provided further support for SUMO1- and SUMO2/3-specific functions in affecting a range of activities including DNA repair, protein turnover, and control of gene expression. For instance, SUMO2/3, but not SUMO1, regulates the LSD1/CoREST/HDAC repressive complex to affect transcriptional changes that are important for cell type–specific gene expression (Ouyang *et al.*, 2009). Similarly, it was reported that SUMO1 and SUMO2 have differential effects on transcription activation of glucocorticoid response genes when fused to the glucocorticoid receptor (Holmstrom *et al.*, 2003). Other lines of evidence supporting nonredundant roles for SUMO1 and SUMO2/3 in regulating cellular functions include their apparent differential activation by cellular stress (Saitoh and Hinchey, 2000; Enserink, 2015), evolution of paralogue-specific E3 ligases and isopeptidases (Cappadocia and Lima, 2018; Kunz *et al.*, 2018), and identification of distinct paralogue-specific substrates through proteomic studies (Hendriks and Vertegaal, 2016). It should be noted that one limitation of many of these studies has been a reliance on the overexpression of exogenous, tagged SUMO paralogues. Collectively, the available data justify a more detailed characterization of SUMO paralogues and their functions.

In this study, we analyzed SUMO paralogue expression levels in human tissues and cell lines using publicly available gene expression data and found supporting evidence for paralogue-specific functions across a wide range of normal human tissues. Using the CRISPR-Cas9 system, we knocked out SUMO1 and SUMO2 paralogue expression individually in human U2OS cells. Systematic analysis of these knockout cell lines revealed unique and nonredundant functions for SUMO1 and SUMO2 in control of cell morphology, stress responses, promyelocytic leukemia (PML) nuclear body assembly, and gene expression. Together, our findings provide insights into unique and nonredundant functions of SUMO1 and SUMO2 in human cells and provide a foundation for further exploration of these functions.

RESULTS

Evaluating SUMO paralogue expression in human tissues and cell lines

Functional contributions of the SUMO paralogues may be reflected in their relative expression levels across various cell lines and tissues. We therefore turned to the Broad Institute's Cancer Cell Line Encyclopedia (CCLE) (Barretina *et al.*, 2012) to explore *SUMO1–5* expression in approximately 500 cancer cell lines derived from bone, breast, liver, lung, ovary, pancreas, and thyroid tissues. *SUMO4* and *SUMO5* were both expressed at either undetectable or very low levels (<1 reads per kilobase of transcript per million reads mapped [RPKM]) in the majority of cell lines (Supplemental Figure 1). Of note, *SUMO5* exists as a processed pseudogene (also known as *SUMO1P1*) whose functionality is uncertain (Liang *et al.*, 2016). In contrast, *SUMO1–3* were expressed at consistently higher levels (1–2 orders of magnitude higher than *SUMO4* and *SUMO5*), with *SUMO2* expression ~37% higher than that of *SUMO1* and *SUMO3*, which had similar levels (Figure 1A). In addition, the relative expression values of the paralogues across cell lines were similar, despite various tissue origins. Because our studies involve U2OS osteosarcoma cells, as described below, we specifically looked at *SUMO1–5* levels in bone cancer cell lines and U2OS cells. Here, we found *SUMO1–3* expression patterns and values consistent with those from the other analyzed cancer cell lines. *SUMO4* was expressed at relatively low levels, and *SUMO5* expression was undetectable (Figure 1B, U2OS in insert).

We next compared *SUMO1–5* gene expression levels in 25 normal human tissues using data from the Genotype-Tissue Expression (GTEx) project. Similar to expression in cancer cell lines, *SUMO4* was expressed at low levels in all analyzed tissues and *SUMO5*
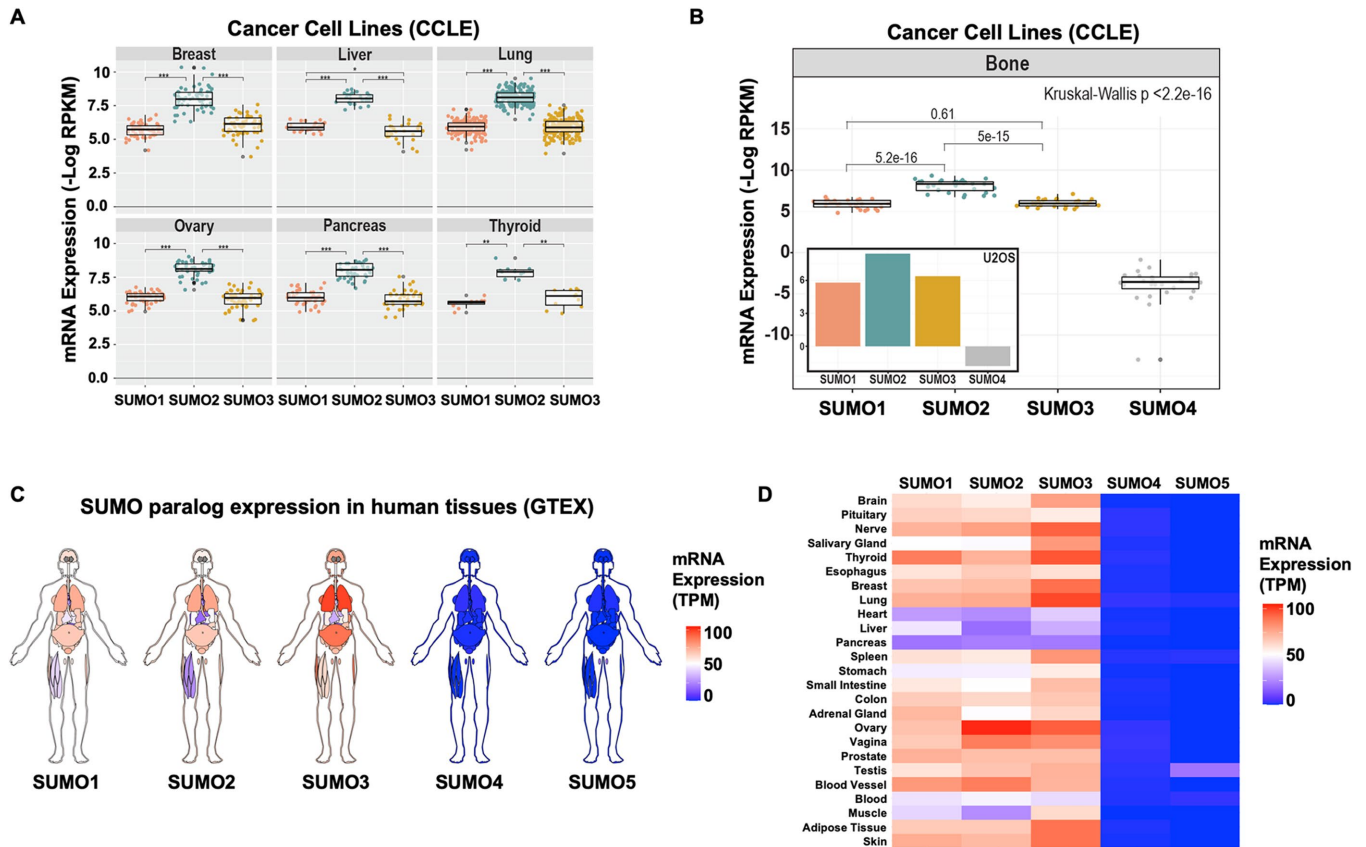
FIGURE 1: SUMO paralogue expression levels vary among human cell lines and tissues. (A) SUMO1–3 mRNA expression ($-\log_{10}$ RPKM) from 467 human cancer cell lines derived from six different tissues. *P* values were determined using a Student's *t* test and are marked with an asterisk (* = 0.027; ** = 2.8e-6; *** < 1.6e-14). (B) SUMO1–4 mRNA expression from 61 human bone cancer cell lines. *P* values were calculated using a Student's *t* test. The inlay shows data from CCLE for the U2OS cell line. *SUMO5* expression was below levels of detection in all bone cancer cell lines. (C) Anatomical heatmaps of SUMO paralogue mRNA expression in normal human tissues. (D) Heatmap of SUMO1 paralogue mRNA expression in normal human tissues. Human data in C and D are from GTEx and are reported in TPM.

expression was below levels of detection in most tissues with several exceptions, including blood and testis (Figure 1D). In contrast, *SUMO1–3* were expressed at consistently higher levels across all tissues analyzed. Of particular interest, relative *SUMO1–3* expression levels varied greatly across tissue and organ types, in contrast to the identical relative expression pattern observed across cancer cell lines (Figure 1C). For instance, we found that *SUMO1* expression was higher than *SUMO2* expression in 15 of the 25 tissues, with the largest difference in expression occurring in the liver, followed by the adrenal gland and muscle (Figure 1D). *SUMO2* expression, however, was higher than that of *SUMO1* in 10 of the 25 tissues, with noticeably elevated levels in reproductive organs, such as the ovaries, vagina, and testis. Finally, *SUMO3* expression levels were higher than those of both *SUMO1* and *SUMO2* in 14 of the 25 analyzed tissues. The various patterns of *SUMO1–3* expression suggest nonredundant functions for these specific paralogues in adult human tissues.

Generation of SUMO1 and SUMO2 KO cells using CRISPR-Cas9

To allow for a more systematic identification and characterization of unique and nonredundant functions of SUMO paralogues in human cells, we used the CRISPR-Cas9 system to individually knock out SUMO1 and SUMO2 expression in U2OS human osteosarcoma

cells. Of the highly similar SUMO2 and SUMO3 paralogues, we chose to focus on SUMO2 given its apparent higher level of expression compared with that of SUMO3 in human cell lines and subsequent supporting evidence that SUMO3 protein levels are low in U2OS cells (Figures 1, A and B, and 2C). We confirmed heterozygous biallelic SUMO gene knockouts (KOs) using Sanger DNA sequencing (Figure 2A). More precisely, we confirmed a deletion of the first exon that interfered with transcription initiation in both alleles of the *SUMO1* gene and the creation of a premature stop codon in the second exon of both *SUMO2* alleles in the respective KO cells (Supplemental Figures 2 and 3).

RNA-sequencing analysis revealed that paralogue mRNA expression patterns in wild-type (WT) U2OS cells were similar to those observed in other cancer cell lines using data from CCLE. Specifically, we found that SUMO2 was the most highly expressed paralogue, followed by SUMO1 and SUMO3 and, finally SUMO4, which had negligible expression (Figure 2B). In the SUMO1 KO cells, *SUMO1* mRNA decreased by >99% as compared with WT values, with a very small increase in *SUMO2* (<3%) and a twofold decrease in *SUMO3*. In the SUMO2 KO cells, we observed a 65% decrease in *SUMO2* signal as compared with WT values. On the basis of observed protein levels (Figure 2C), we hypothesize that the higher-than-expected levels of *SUMO2* mRNA may be due to detection of mutant transcripts. Also of note, we observed a 17% increase in
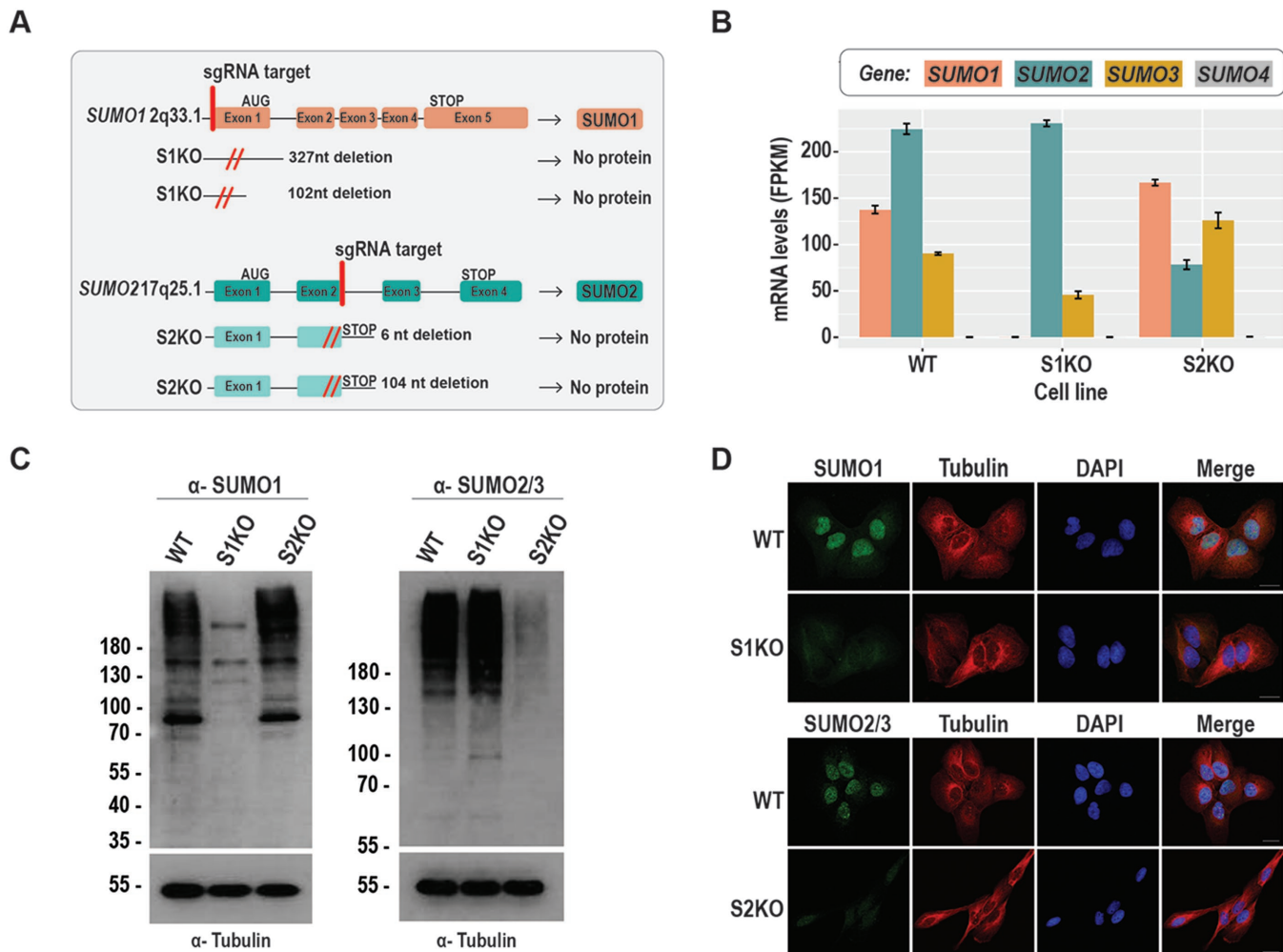
FIGURE 2: Generation and validation of SUMO KO cell lines. (A) Schematic of CRISPR-Cas9 knockout strategy and sequencing results. (B) SUMO paralogue mRNA expression levels in WT and KO cells, measured by RNA-seq. (C) Immunoblots of WT and KO whole cell lysates show a significant reduction in SUMO1 and SUMO2/3 conjugated proteins in respective KO cells, with tubulin used as a loading control. (D) Immunofluorescence microscopy images reveal loss of SUMO1- or SUMO2/3-specific signal in respective KO cells. Tubulin costaining reveals changes in cellular morphology.

SUMO1 and a 63% increase in *SUMO3* mRNA expression in the SUMO2 KO cells. Despite this increase in *SUMO3* transcript, however, SUMO3 protein levels were relatively low as determined by immunoblotting and immunofluorescence microscopy (see below).

To evaluate SUMO1 and SUMO2/3 protein expression in the KO cells, we performed immunoblot and immunofluorescence microscopy assays with SUMO1- and SUMO2/3-specific antibodies. Both assays revealed undetectable levels of SUMO1-modified proteins and severely diminished levels of SUMO2/3-modified proteins in the respective KO cell lines (Figure 2, C and D). Because the SUMO2/3 antibody recognizes an epitope common to both SUMO2 and SUMO3 (Becker *et al.*, 2013), residual signal in the SUMO2 KO cells is a likely indicator of the relatively low level of SUMO3 protein expression. Quantitative analysis of immunofluorescence images revealed that SUMO3 is expressed at approximately 20% of the levels of the combined SUMO2/3 expression in wild-type cells (Supplemental Figure 4). Taken together, we generated viable cell lines with undetectable levels of SUMO1 protein expression and severely reduced levels of SUMO2/3 expression.

Characterization of morphological changes of SUMO KO cells

Immunofluorescence microscopy revealed unique changes in the morphology of SUMO2 KO cells as compared with WT and SUMO1 KO cells. Specifically, ~50% of SUMO2 KO cells exhibited a fibroblast-like morphology with an elongated and bipolar shape that contrasted with the primarily polygonal and epithelial-like WT and SUMO1 KO cells (Figure 2D). Notably, fewer than 5% of WT and SUMO1 KO cells exhibited a fibroblast-like morphology (Figure 3A). To investigate whether the change in morphology was due specifically to the loss of SUMO2, we constructed SUMO2 KO rescue cell lines with stable, constitutive SUMO2 reexpression or SUMO1 overexpression by plasmid transfection and single-cell cloning. SUMO2 and SUMO1 protein levels in the rescue cell lines (S2KO+S2 and S2KO+S1, respectively) were assessed by immunoblotting and immunofluorescence microscopy (Figure 3, B and C). Semiquantitative measurements of relative SUMO protein levels revealed a near complete restoration of SUMO2/3 expression in the S2KO+S2 cells and a nearly twofold increase in SUMO1 expression in the S2KO+S1 cells as compared with endogenous levels in WT cells (Supplemental
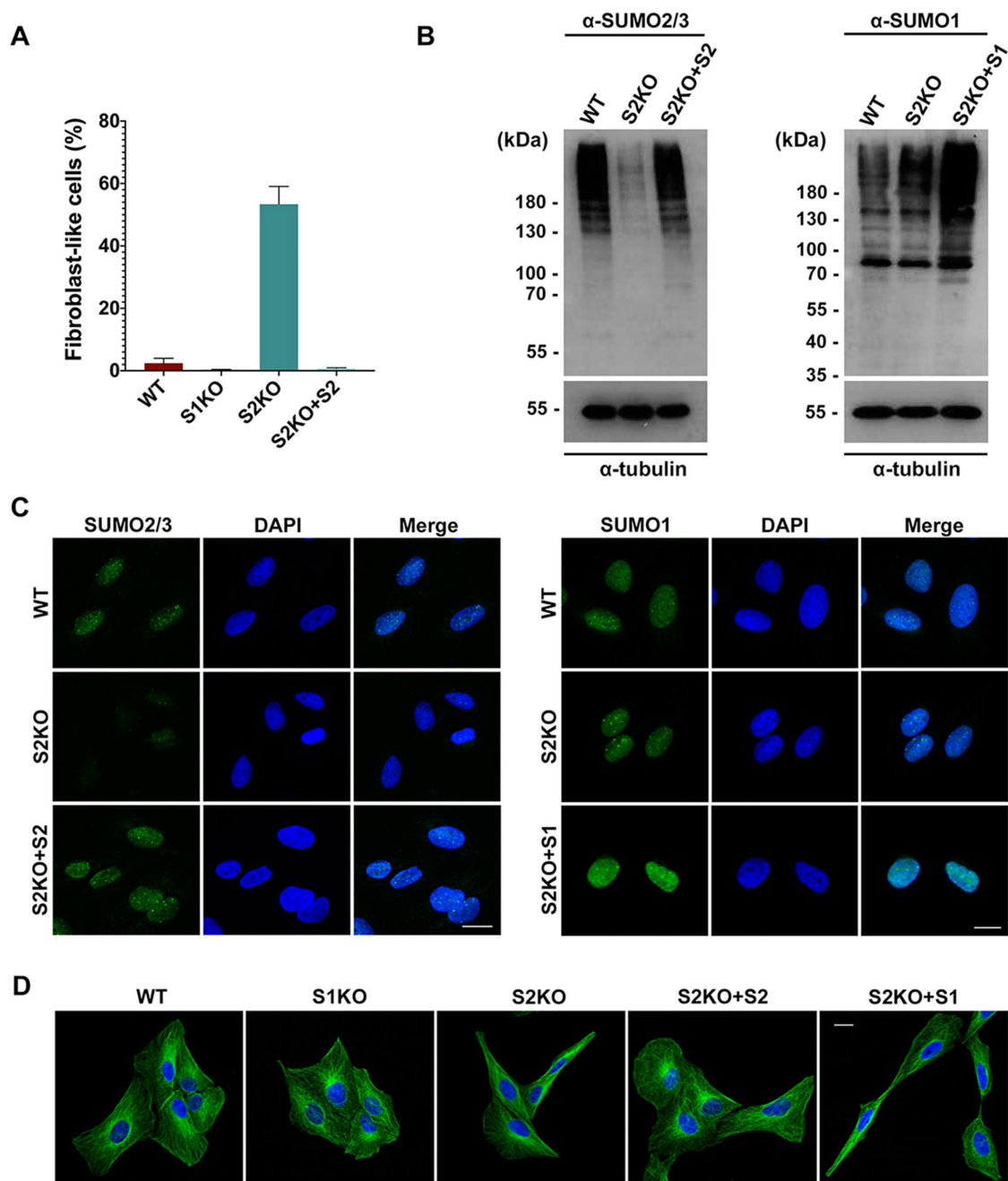
FIGURE 3: SUMO2 has a unique role in regulating cellular morphology. (A) Percentage of fibroblast-like cells in the indicated cell lines. More than 2400 cells from three independent experiments were analyzed by immunofluorescence microscopy for each cell line. (B) SUMO2 reintroduction in S2KO+S2 cells and SUMO1 overexpression in S2KO+S1 cells were validated by immunoblotting using specific antibodies. Tubulin was used as a loading control. (C) Expression levels of SUMO2/3 and SUMO1 were assessed by immunofluorescence microscopy with specific antibodies and DAPI counterstaining. (D) Morphology of the indicated cell lines was analyzed by anti-tubulin immunofluorescence microscopy with DAPI counterstaining. Scale bars: 20 µm.

Figure 5). A visual inspection of the rescue cell lines by immunofluorescence microscopy revealed that reintroduction of SUMO2 appeared to restore the epithelial-like morphology of WT cells, whereas SUMO1 overexpression had no effect (Figure 3, A and D).

To quantitatively assess the morphological changes of the knockout and rescue cell lines, we used FIJI image processing software (Schindelin *et al.*, 2012) to analyze the average aspect ratio, area, and circularity of the cells. Consistent with our visual inspection, quantitative measurements revealed a nearly twofold increase in the approximate length-to-width ratio (aspect ratio, 3.30 vs. 1.77 vs. 1.63) of SUMO2 KO cells as compared with WT and SUMO1 KO cells, respectively. Additionally, we observed a decrease in the average cell area (1092 µm^2 vs. 1705 µm^2 vs. 1710 µm^2) and circularity (0.46 vs. 0.63 vs. 0.70) of the SUMO2 KO cells compared with WT and SUMO1 KO cells (Figure 4A). No significant differences were observed in the average aspect ratio or cell area between SUMO1 KO and WT cells, although SUMO1 KO cells were slightly more circular in comparison to WT cells. Further assessment of the rescue
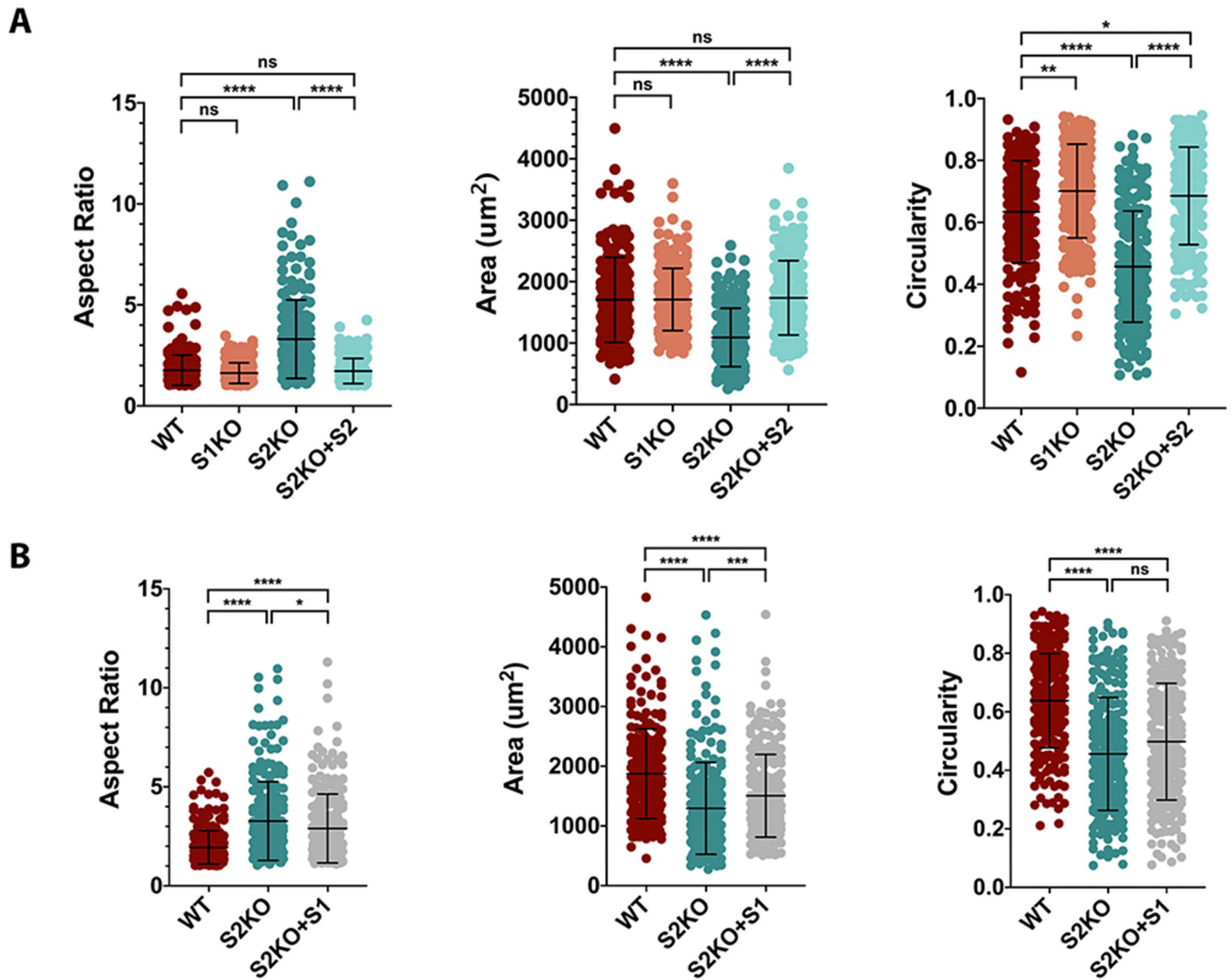
FIGURE 4: Rescue of S2KO cells reveals paralogue-specific functions of SUMO2 in regulating U2OS cell morphology. (A) Quantitative shape analysis was performed using FIJI and Prism (see *Materials and Methods*) revealing changes in the average cellular aspect ratio, area, and circularity in the indicated cell lines. More than 200 cells from three independent experiments were analyzed for each cell line. Error bars represent SDs. *P* values were calculated by a Kruskal–Wallis test using Prism software; **** $p \leq 0.0001$, *** $p \leq 0.001$, * $p \leq 0.05$, ns $p > 0.05$. (B) Aspect ratio, area, and circularity of WT, S2KO, and S2KO+S1 cell lines, analyzed as in A.

cell lines confirmed that reintroducing SUMO2 rescued the morphology changes. Changes in aspect ratio and area were also observed in S2KO overexpressing SUMO1, although the effects were less pronounced (Figure 4B). Collectively, these results reveal a unique and paralogue-specific function for SUMO2 in regulating cellular morphology.

Cell cycle analysis of SUMO KO cells
Previous studies have shown that SUMO1 and SUMO2/3 have unique associations with mitotic chromosomes and that sumoylation of key mitotic regulators is required for timely cell cycle progression (Joseph *et al.*, 2002; Dasso, 2008; Zhang *et al.*, 2008b; Mukhopadhyay *et al.*, 2010; Cubenas-Potts *et al.*, 2013; Cubenas-Potts *et al.*, 2015; Lee *et al.*, 2018). We therefore used flow cytometry to gain insights into possible differences in the cell cycle dynamics of WT and SUMO KO cells. Using this approach, we found a nearly identical distribution of cells in the G0/G1, S, and G2/M phases of the cell cycle in WT, SUMO1, and SUMO2 KO cell lines (Figure 5A). Of inter-

est, we detected a population of cells that had a greater than 2N DNA content specifically in the SUMO2 KO cells. Quantitative analysis revealed that this population of >2N cells was significantly higher in the SUMO2 KO cells as compared with WT, whereas no other significant differences between cell lines were identified (Figure 5B).

Characterization of PML-NBs in SUMO KO cells
Sumoylation has important roles in regulating the assembly and function of PML nuclear bodies (PML-NBs) (Seeler and Dejean, 2001; Lallemand-Breitenbach and de The, 2018). In particular, sumoylation is thought to affect the phase separation of proteins that underlies the formation of these membraneless organelles (Banani *et al.*, 2016), though the individual functions of SUMO1 and SUMO2 in this process are less clear. We therefore analyzed the number and size of PML-NBs in WT and SUMO KO cells using antibodies specific for PML and another resident PML-NB protein, DAXX, coupled with immunofluorescence microscopy. Consistent with nonredundant
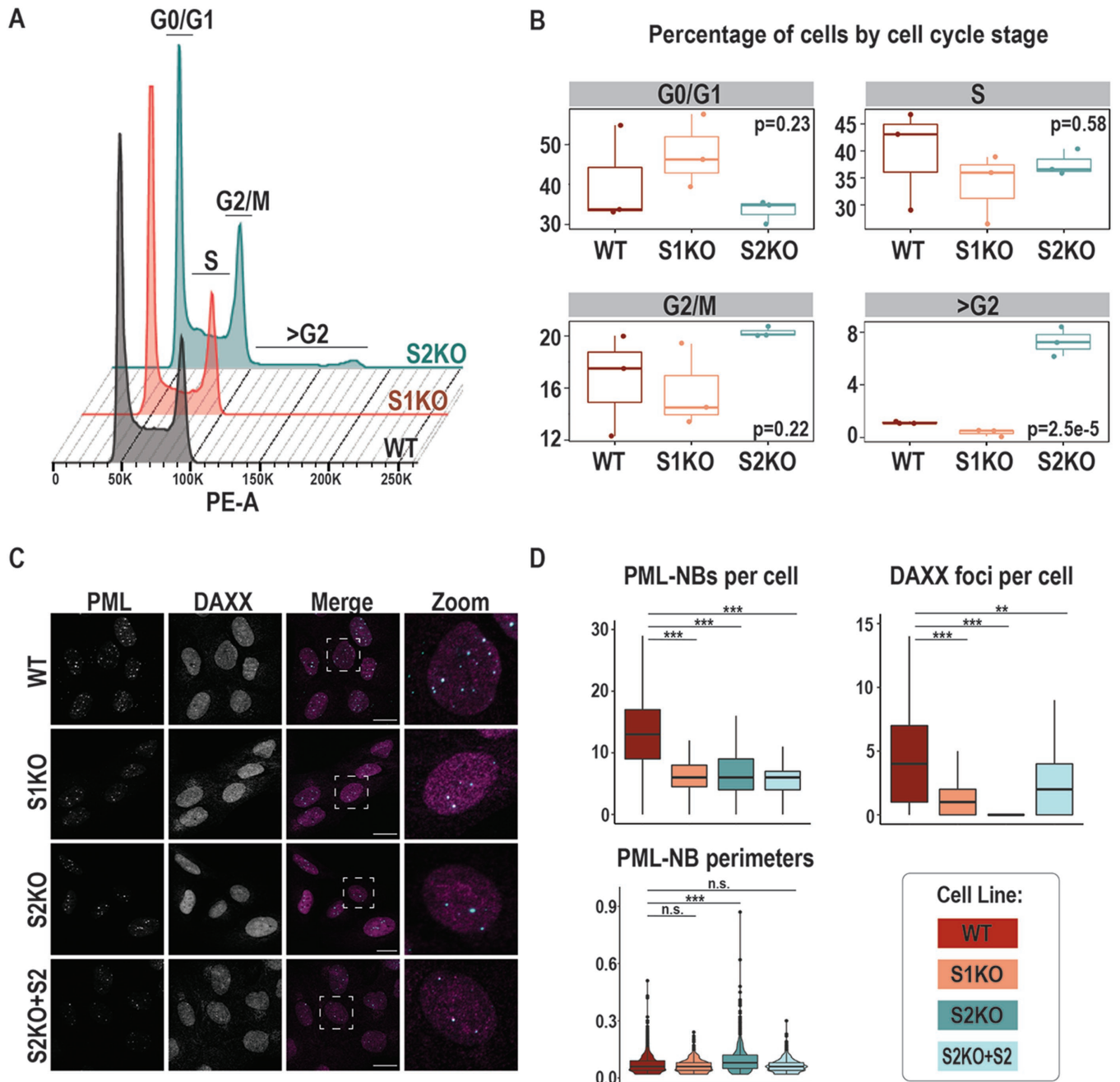
FIGURE 5: Cell cycle and nuclear body analysis of SUMO KO cells. (A) Overlay of WT, S1KO, and S2KO histograms from flow cytometry analysis. (B) Quantification of the percentage of WT, S1KO, and S2KO cells in G0/G1, S, G2/M, and >G2 cell cycle stages. Indicated *p* values were calculated using an ANOVA. (C) Immunofluorescence microscopy images using antibodies specific for PML and DAXX. (D) Quantification of PML-positive nuclear bodies (PML-NBs), DAXX-positive NBs, and PML-NB perimeter size estimates for each cell line; an average of 180 cells were analyzed for each cell line from two independent experiments. *P* values for each cell line as compared with WT were calculated using an unpaired Wilcoxon test (ns = not significant, ** $p = 1 \times 10^{-8}$, and *** $p < 2.2 \times 10^{-16}$).

roles for the paralogues in PML-NB assembly and function, we observed a significant decrease in the number of nuclear bodies detected with both PML and DAXX in the SUMO1 and SUMO2 KO cells (Figure 5, C and D). In agreement with the literature (Lallemand-Breitenbach and de The, 2010), we observed a mean of approximately 13–14 PML-positive foci per nucleus in WT cells, with a reduction to approximately 6–7 in SUMO1 and SUMO2 KO cells per nucleus (Figure 5D). Moreover, although DAXX was detected only in a subset of PML-NBs, a similar decrease in DAXX-positive foci was observed in the KO cells as compared with WT. Specifically, an average of 4–5 DAXX-positive foci were detected per nucleus in WT cells, whereas only 1–2 foci were detected in SUMO1 KO cells and 0–1 per nucleus in SUMO2 KO cells. Surprisingly, the decrease in PML-positive foci in SUMO2 KO cells was not rescued by reintroducing SUMO2 expression, whereas the number of DAXX positive foci was partially restored (Figure 5D). These findings reveal nonredundant roles for SUMO1 and SUMO2 in affecting PML-NB assembly or integrity and suggest that loss of SUMO function may have

irreversible effects on factors underlying their number and size. Further studies are needed to determine whether the observed decrease in NBs is due to lack of formation of PML-NBs, or whether the stability is compromised in the absence of SUMO1 and SUMO2.

Characterization of cellular stress responses in SUMO KO Cells

MTT assays and mitochondrial function. Sumoylation has important functions in regulating cellular stress responses (Enserink, 2015). To investigate the individual requirements for SUMO1 and SUMO2 in response to cellular stressors, we challenged WT, SUMO1 KO, and SUMO2 KO cells with a variety of stress conditions and measured cell survival using an 3-[4,5-dimethylthiazol-2-yl]-2,5-diphenyl tetrazolium bromide (MTT) assay. The MTT assay measures the activity of mitochondrial NAD(P)H-dependent oxidoreductase enzymes and thus provides a quantitative readout of mitochondrial respiration and cell viability (van Meerloo *et al.*, 2011). We first validated the MTT assay for linearity and found that the readout is a linear function of cell number for WT and SUMO KO cells (Figure 6A). We also noted, however, that the MTT readout for the SUMO2 KO cells was consistently lower compared with that for WT and SUMO1 KO cells. Taking advantage of the SUMO2 rescue cell lines described above, we found that reintroduction of SUMO2 partially rescued the reduced MTT signal of SUMO2 KO cells, whereas overexpression of SUMO1 increased the signal above WT values (Figure 6A). These findings suggest that SUMO1 and SUMO2 may have unique and nonredundant roles in regulating the number or function of mitochondria.

Proteotoxic stress responses. To investigate the functions of SUMO1 and SUMO2 in response to proteotoxic stress, we treated cells with various doses of two different drugs, azetidine-2-carboxylic acid (AZC) and eeyarestatin I (EerI). AZC is a proline amino acid analogue that causes protein misfolding when incorporated into newly synthesized polypeptides (Zagari *et al.*, 1990). WT and SUMO KO cells were treated with various doses of AZC for 72 h, and cell viability was measured using the MTT assay (Figure 6B). We observed a dose-dependent decline in WT cell viability, demonstrating drug toxicity, and similar dose-dependent declines were also observed in SUMO1 and SUMO2 KO cells. These findings suggest that the SUMO paralogues do not have an obvious effect on the response to protein misfolding caused by AZC or that SUMO1 and SUMO2 are functionally redundant in this response.

EerI is an inhibitor of protein translocation into the endoplasmic reticulum (ER), in part through inhibition of Sec61 and the p97 AAA+ ATPase (Wang *et al.*, 2008, 2010). It also inhibits ER-associated degradation (ERAD), which targets misfolded proteins in the ER for degradation through the ubiquitin proteasome pathway (McKibbin *et al.*, 2012; Brem *et al.*, 2013). Treatment of cells with EerI leads to the accumulation of ubiquitylated proteins in the cytoplasm, but whether sumoylation also plays a role in the response to EerI has not been previously tested. We first treated WT cells with EerI for various lengths of time and evaluated the effects on SUMO conjugates by immunoblot analysis (Figure 6C). We detected an apparent increase in free, unconjugated SUMO1, but no obvious increases in high-molecular-mass SUMO1 conjugates. In contrast, an increase in high-molecular-mass SUMO2/3 conjugates was detected at 2 and 4 h of treatment, indicating that Eer I-induced stress enhances SUMO2/3 modification. To further evaluate functional requirements in the response to Eer1-induced stress, we treated WT and SUMO KO cells with various doses of EerI for 48 h and viability was measured using the MTT assay (Figure 6D). SUMO2 KO cells were uniquely sensitive

to EerI, and sensitivity was most pronounced at 2 µM, where SUMO2 KO cell viability was reduced to 30%, compared with ~60% in WT and SUMO1 KO cells. To investigate whether sensitivity to EerI was due specifically to the loss of SUMO2, we performed dose-response assays using SUMO2 KO rescue cell lines. Surprisingly, reintroduction of SUMO2 and overexpression of SUMO1 both rescued the enhanced sensitivity of SUMO2 KO cells to EerI. Thus, differences in the relative expression levels of SUMO1 and SUMO2 may influence their roles in the cellular response to EerI.

Genotoxic stress responses. To study the functions of SUMO1 and SUMO2 in response to genotoxic stress, we investigated the sensitivity of WT and SUMO KO cells to treatment with hydroxyurea (HU), a drug that inhibits ribonucleotide reductase and causes DNA replication arrest and double-strand breaks (Singh and Xu, 2016). Cells were treated with various doses of HU for 72 h, and viability was measured using the MTT assay. This analysis revealed that SUMO1 and SUMO2 KO cells were similarly less sensitive to HU as compared with WT cells (Figure 6E). SUMO1 and SUMO2 KO cells showed equal resistance at doses of HU below 400 µM, whereas SUMO2 KO cells exhibited slightly greater resistance at doses above 400 µM. The reduced sensitivity of SUMO2 KO cells to HU was rescued by reintroducing SUMO2 but not by overexpressing SUMO1 (Figure 6E). These findings indicate that SUMO1 and SUMO2 have nonredundant functions in promoting cell survival in the presence of HU-induced DNA replication stress.

Finally, the reduced toxicity of HU may be due to mechanisms that limit its effect on nucleotide biosynthesis and DNA replication arrest or on mechanisms that operate downstream of replication arrest. To distinguish between these possibilities, we assessed the effect of HU treatment on cell cycle progression by measuring cell growth over 4 d in the presence or absence of 700 µM HU (Figure 6F). Compared with untreated cells, which all exhibited exponential growth, all treated cells showed a near-complete inhibition of proliferation at 1 and 2 d of exposure. Thus, WT and SUMO KO cells exhibited similar cell cycle arrests at early time points of HU treatment, consistent with the expected inhibition of DNA replication. This indicates that the reduced sensitivity of SUMO KO cells to HU is due to effects downstream of replication arrest. Notably, SUMO2 KO cells were unique in displaying detectable proliferation at days three and four of HU exposure, suggesting a possible paralogue-specific defect in sustaining DNA damage checkpoints.

Transcriptomics profiling of SUMO KO cells

Numerous studies have examined how sumoylation of transcription factors and chromatin remodeling proteins affects expression of target or reporter genes (Gill, 2005; Cubenas-Potts and Matunis, 2013; Rosonina *et al.*, 2017); however, there are limited data on the global effects of SUMO paralogues on gene expression. To address this gap in knowledge, we analyzed the effects of SUMO1 and SUMO2 knockout on the transcriptome of U2OS cells.

Summary of findings and validation of results. Using RNA sequencing (RNA-seq), we identified a combined total of 10,336 genes that were differentially expressed in SUMO1 and SUMO2 KO cells as compared with WT (Figure 7A). These differentially expressed genes (DEGs) account for a remarkable 70% of all identified genes. Of the identified DEGs, 42% (4343 genes) were uniquely affected in SUMO2 KO cells and 20% (2068 genes) were unique to the SUMO1 KO cells (Figure 7A). Despite the differences in the number of affected genes, nearly equal numbers of DEGs were up- and down-regulated in each cell line. Collectively, these findings are
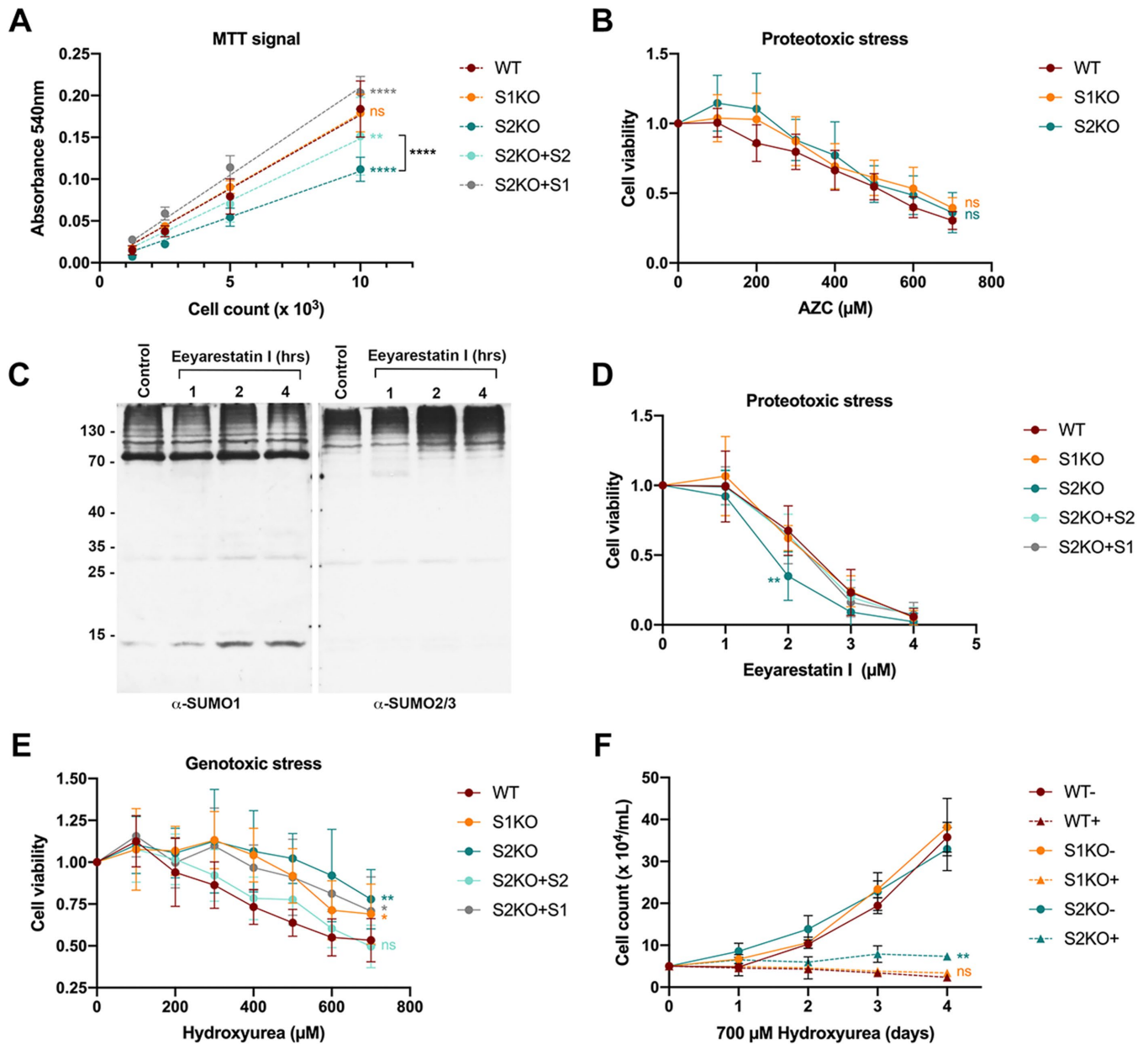
FIGURE 6: SUMO paralogues have nonredundant functions in stress responses. (A) Baseline linear readout of MTT assay signal for the indicated numbers of WT and KO cell lines. Simple linear regressions were calculated for each cell line: $R^2 = 0.91$ (WT), 0.96 (S1KO), 0.94 (S2KO), 0.81 (S2KO+S2), and 0.96 (S2KO+S1). (B) Cells were treated with the indicated doses of AZC for 72 h, and cell viability was determined using an MTT assay. (C) WT cells were treated with 8 μm EerI for the indicated times, and cell lysates were analyzed by immunoblotting with SUMO1- or SUMO2/3-specific antibodies. (D) Cells were treated with the indicated doses of EerI for 48 h, and cell viability was determined using an MTT assay. (E) Cells were treated with the indicated doses of HU for 72 h, and cell viability was determined using an MTT assay. Relative cell viability was calculated in B, C, and E as the fraction of MTT signal at each drug dosage compared with untreated control cells. (F) Cells were treated with (dashed line, +) or without (solid line, –) 700 μM HU for up to 4 d. Viable cells were counted at each time point and plotted. Error bars equal SDs, $n = 3$. (**** $p \le 0.0001$, *** $p \le 0.001$, * $p \le 0.05$, ns $p > 0.05$).

consistent with sumoylation playing a profound role in affecting gene expression and provide evidence that SUMO1 and SUMO2 perform unique and nonredundant functions that affect both activation and repression of different subsets of genes.

To help focus our analysis, we tightened the significance threshold to include only genes with a $\log_2$ fold change ≥2 (equivalent to a fourfold change). This more stringent parameter resulted in a combined total of 861 DEGs and highlighted a more prominent role for

SUMO2 in affecting gene expression, as 95% of these DEGs were unique to the SUMO2 KO cells (Figure 7A). Consistently, many DEGs with the greatest fold changes in SUMO1 KO cells overlapped with SUMO2 KO cells (Figure 7B).

To validate our RNA-seq findings, we selected a subset of up- and down-regulated DEGs and tested gene expression by real-time quantitative reverse transcription PCR (qRT-PCR). We found a strong correlation ($R^2 > 0.9$) between the assays for both SUMO KO cell
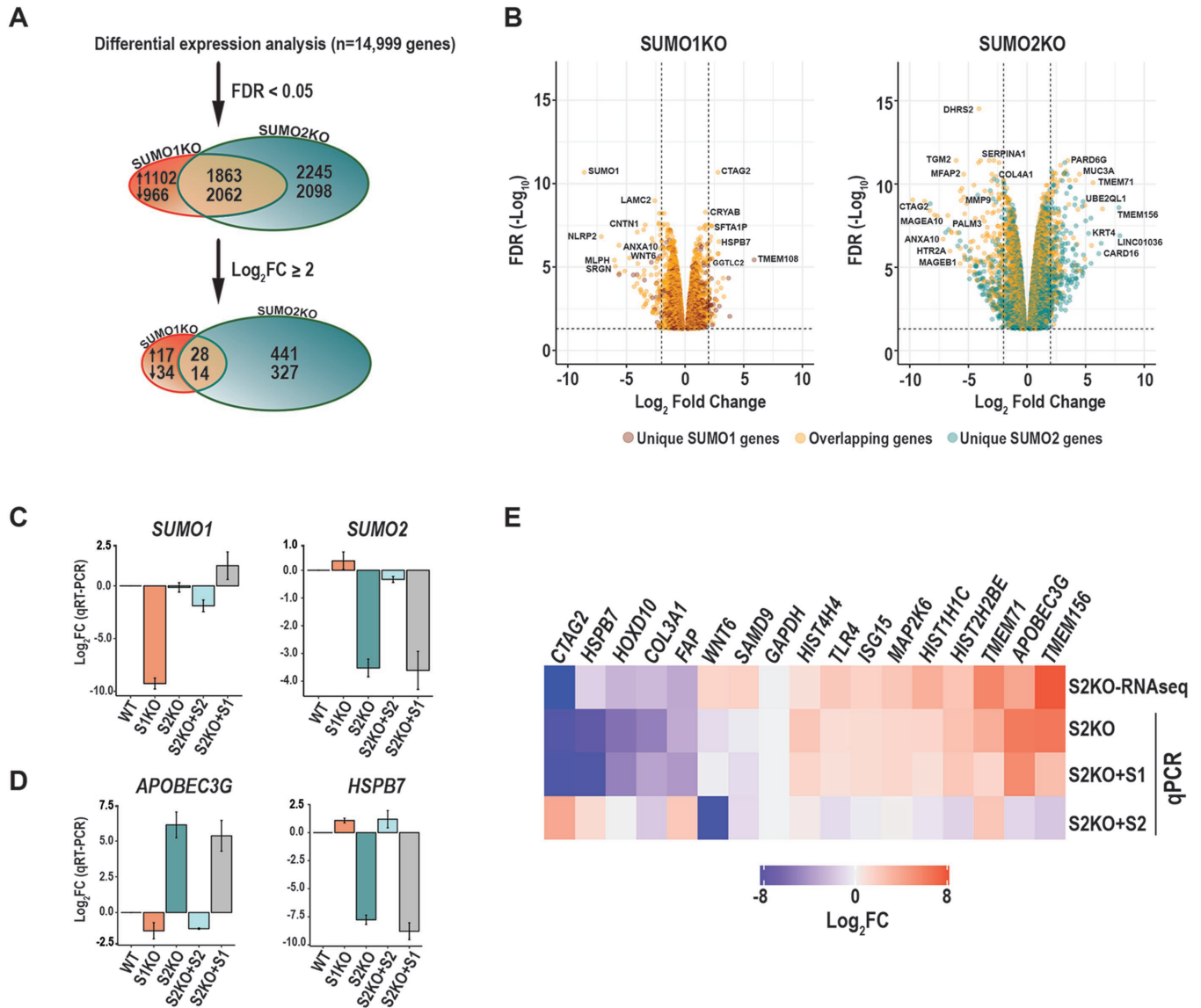
FIGURE 7: SUMO1 and SUMO2 uniquely regulate gene expression. (A) Venn diagram showing the numbers of unique and overlapping up-regulated and down-regulated DEGs in the S1KO and S2KO cells, at two significance thresholds, FDR < 0.05 and FDR < 0.05 + Log$_2$ fold change (FC). (B) Volcano plots of unique and overlapping SUMO1 and SUMO2 KO cell DEGs. The horizontal dashed line represents FDR < 0.05, and the vertical dashed lines represent Log$_2$FC values of −2 and +2. (C) SUMO1 and SUMO2 gene expression values by qRT-PCR in WT, KO, and rescue cell lines. (D) Representative bar plots of Log$_2$FC expression values of up- and down-regulated genes, tested by qRT-PCR. (E) Heatmap summarizing SUMO2 KO and rescue cell line Log$_2$FC values for genes tested by RNA-seq and qRT-PCR (all graphs shown in Supplemental Figure 8).

lines (Supplemental Figure 7E). To further validate that the robust gene changes observed in SUMO2 KO cells were due specifically to the loss of SUMO2, we also analyzed gene expression levels in both of the SUMO2 KO rescue lines (S2KO+S2 and S2KO+S1) by qRT-PCR. We first used qRT-PCR to quantify SUMO1 and SUMO2 mRNA levels in all tested cell lines to confirm SUMO1 and SUMO2 reexpression in the rescue lines (Figure 7C). We then analyzed 16 DEGs and found that expressing SUMO2 in the SUMO2 KO (S2KO+S2) cells resulted in near-WT levels of gene expression. Interestingly, expression values in the S2KO+S2 cells often went beyond WT values and in the opposite direction of the SUMO2 KO cells (Figure 7, D and E, and Supplemental Figure 8), suggesting that SUMO2 has a strong effect on the expression of these genes. Further in support of the observed gene expression changes resulting from a direct

loss of SUMO2, we also found that gene expression values were not rescued when SUMO1 was overexpressed in SUMO2 KO cells (S2KO+S1) (Figure 7, C–E). Moreover, gene expression levels from these cells were nearly indistinguishable from that in SUMO2 KO cells, demonstrating that SUMO1 is unable to compensate for the loss of SUMO2 in regulating gene expression.

Karyoplot analysis. To identify possible patterns or clusters of genes affected by the loss of SUMO1 and SUMO2, we next mapped the DEGs that had a >4-fold change in expression to the human genome (Figure 8, A and B). SUMO1 KO DEGs were randomly scattered throughout the genome, with the exception of genes clustered near the end of chromosome 2 and a cluster of histone genes on chromosome 6. Notably, these and other more significantly
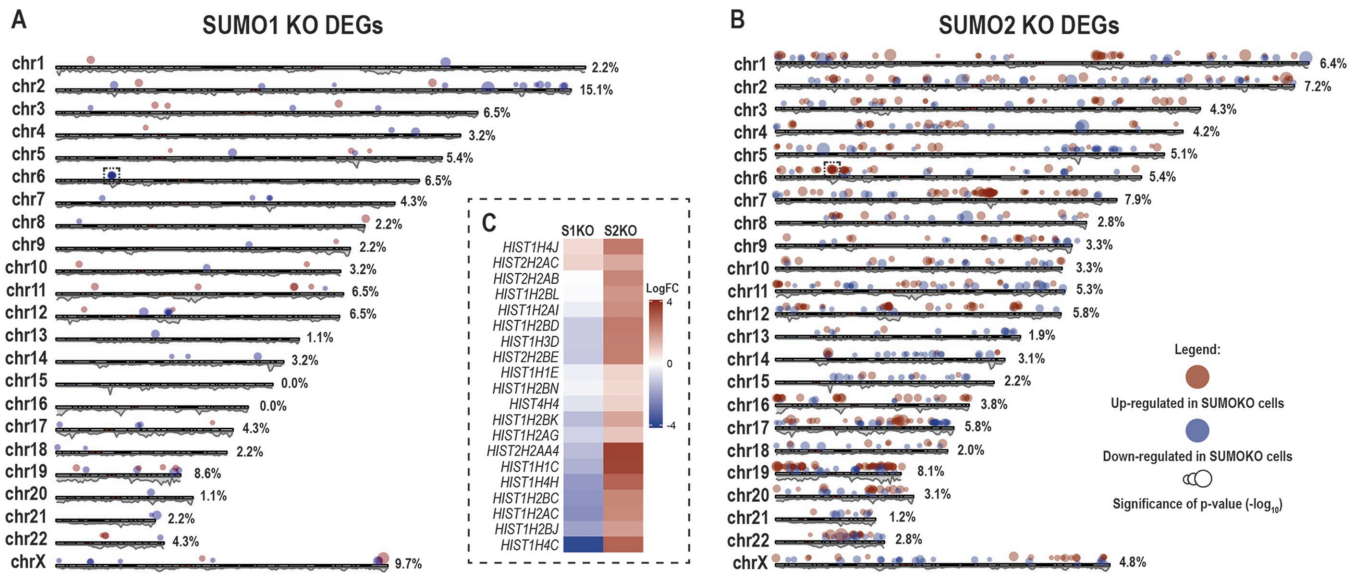
FIGURE 8: SUMO KO cell DEGs are localized throughout the genome. (A) Genomic locations of up- and down-regulated genes from the SUMO1 KO cells are mapped to their genomic loci. The gray plot below each chromosome represents gene density across each chromosome. The percent of DEGs per chromosome is labeled to the right of each chromosome: (# of DEGs on the chromosome/total # of DEGs) × 100. (B) Same as in A, but for SUMO2 KO cell DEGs. (C) Corresponding heatmap of histone gene expression as measured by RNA-seq.

affected DEGs in the SUMO1 KO cells were down-regulated, as represented by the larger blue dots on the karyoplot. In contrast, SUMO2 KO cell DEGs were more equally up- and down-regulated. In addition, "hotspots" of up- and down-regulated SUMO2 KO DEGs were observed throughout the genome, including the same histone gene cluster on chromosome 6 that was observed in SUMO1 KO cells. Closer examination of these histone genes revealed opposing effects of SUMO1 and SUMO2, as they were down-regulated in the SUMO1 KO cells but up-regulated in the SUMO2 KO cells (Figure 8C). Finally, we found that the SUMO2 KO DEGs often occurred at regions of high gene density, as represented by the gray density plot under each chromosome, whereas there was no such clear association with SUMO1 KO DEGs. Of note, DEGs identified in SUMO1 and SUMO2 KO cells were equally distributed between positive and negative sense strands of the genome and among genes of various lengths.

Gene set enrichment analysis. To explore the cellular functions associated with genes affected by the loss of SUMO1 or SUMO2, we turned to the Broad Institute's Gene Set Enrichment Analysis (GSEA) (Subramanian *et al.*, 2005). Significantly enriched gene sets were characterized into five broad categories: nucleus-related, transcription and signaling, cellular stress response, immune response, and cell morphology (Figure 9A). Intriguingly, although a majority of these gene sets were enriched in both the SUMO1 and SUMO2 KO cells, the same gene sets often contained genes with opposing expression levels. For instance, histone modification gene sets were heavily enriched with down-regulated genes in the SUMO1 KO cells (blue dots) and up-regulated genes in the SUMO2 KO cells (red dots). This is in line with our previous observation that histone gene expression decreases in SUMO1 KO cells yet increases in SUMO2 KO cells and further reveals that the paralogues can have opposing effects on gene expression.

A similar trend of shared gene sets with opposing expression levels was also observed for the transcription and signaling, cellular stress response, and immune response categories. The immune

response categories were of particular interest in light of recent discoveries highlighting the importance of sumoylation in the immune response (Adorisio *et al.*, 2017). Consistent with the literature, we found an enrichment in innate immune response gene sets, such as interferon (IFN) α and γ responses, interleukin-signaling, and viral genome integrity. A closer look at the data revealed that a majority of IFN-α response genes are up-regulated in the SUMO2 KO cells. These same genes were also mostly up-regulated in the SUMO1 KO cells, but to a lesser extent (Figure 9B). Conversely, IFN-γ response genes are almost all down-regulated in the SUMO1 KO cells but have mixed expression in the SUMO2 KO cells (Figure 9B).

Finally, cell morphology–related gene sets were of interest because of the previously described cell morphology phenotype observed uniquely in the SUMO2 KO cells. Notably, individual gene sets in this category, including the extracellular matrix, collagen formation, and epithelial-to-mesenchymal gene sets, were uniformly down-regulated in the SUMO2 KO cells (Figure 9B). Taken together, these findings reveal that SUMO1 and SUMO2 have unique and nonredundant roles in regulating a broad range of genes. Moreover, they reveal a dominant role for SUMO2 in regulating gene expression and opposing the effects of SUMO1 and SUMO2 on expression of identical genes.

DISCUSSION
Vertebrates express five SUMO paralogues whose individual functions remain to be fully understood. In this study, we provide evidence for nonredundant paralogue-specific functions through informatic analysis of gene expression data from human tissues and experimental analysis of SUMO1 and SUMO2 KO cell lines. Our gene expression analysis revealed that relative mRNA levels of SUMO1, SUMO2, and SUMO3 vary across tissues, indicative of tissue-specific functions. Systematic analysis of the SUMO1 and SUMO2 KO cells revealed paralogue-specific phenotypes that included various responses to cellular stress, unique gene expression patterns, and nonredundant roles in nuclear body integrity. Moreover, we observed morphological changes that were unique to the
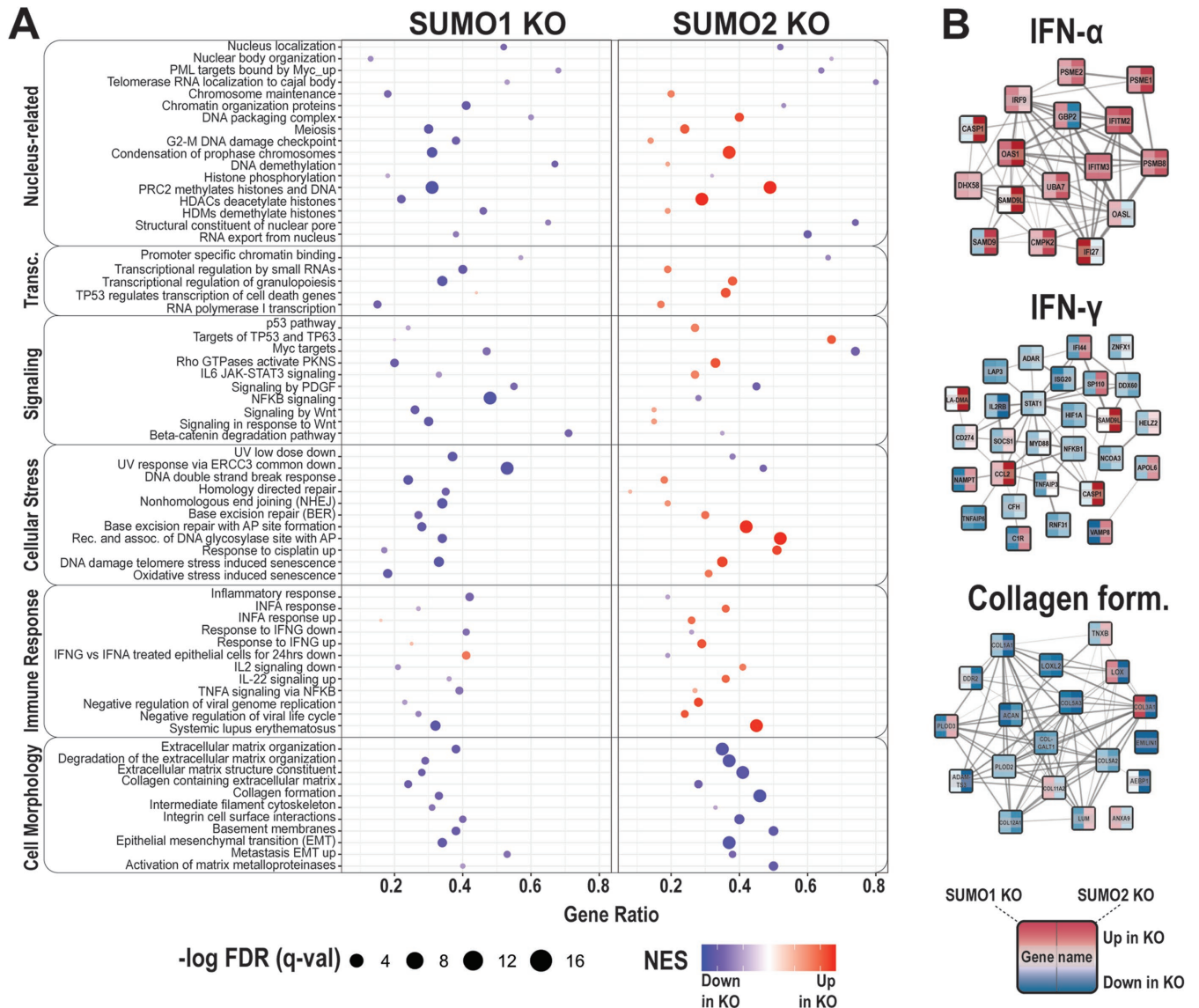
FIGURE 9: SUMO paralogues have opposing roles on gene expression. (A) GSEA results showing enriched gene sets for S1KO and S2KO cell lines as grouped into six broad categories. Abbreviations: Transc. = transcription, NES = normalized enrichment signal. (B) Cytoscape-STRING protein interaction networks for IFN-α, -γ, and collagen formation processes.

SUMO2 KO cells. Reexpression of SUMO2 in the SUMO2 KO cells rescued the morphology, gene expression, and response to genotoxic and proteotoxic stress phenotypes. In contrast, overexpression of SUMO1 did not rescue these phenotypes. Collectively, these findings demonstrate that SUMO1 and SUMO2 have nonredundant biological activities that are determined by unique molecular properties. Additionally, the significant transcriptional changes observed in the KO cells underscore the potential for SUMO1 and SUMO2 to regulate cellular processes through a complex combination of effects on gene expression and control of relevant downstream regulatory and structural proteins.

Tissue-specific SUMO paralogue functions

Of particular interest, our SUMO paralogue expression analysis across human tissues and cell lines revealed an unexpected dichotomy; relative paralogue expression levels were universally the same across hundreds of cell lines (regardless of tissue source), whereas variable relative expression levels were detected across tissues.

Moreover, the relative levels of SUMO3 expression were surprisingly high in many tissues in contrast to cell lines. We note, however, that our analysis in U2OS cells revealed that levels of SUMO3 protein produced from available mRNA transcripts is low in comparison to those of SUMO1 and SUMO2 (Figure 2, B and C). This is consistent with findings that correlations between mRNA and protein products of different genes can vary widely (Gry *et al.*, 2009). Thus, it will be important to investigate SUMO paralogue protein levels in tissues to fully understand their relative functional contributions. Nonetheless, these findings suggest that the cellular environment strongly influences SUMO paralogue expression levels and that cells in culture adopt expression levels optimized for in vitro growth conditions. The relatively limited number of studies analyzing SUMO expression and function in tissues, including mouse retina, brain, and human placenta, are consistent with complex patterns of expression and predicted functions (Gong and Li, 2010; Hasegawa *et al.*, 2014; Baczyk *et al.*, 2018; Karhausen *et al.*, 2018). Thus, while fundamentally important insights into SUMO paralogue-specific functions may

be inferred from cell culture–based studies like those reported here, the findings suggest that a full appreciation and understanding of their functions will require additional experimentation at the tissue and organismal levels.

The complexity of observed SUMO KO phenotypes

SUMO1 and SUMO2 can be conjugated to more than 1000 different proteins, some overlapping and also some unique to each paralogue (Hendriks and Vertegaal, 2016). It can therefore be anticipated that observed phenotypes are multifactorial, involving changes in the posttranslational modification of more than one protein, and also proteins functioning at multiple different levels. The change in cell morphology observed in SUMO2 KO cells provides a prime example of how disrupting the regulation of multiple proteins functioning at multiple levels could converge to produce this particularly striking phenotype. Sumoylation has, for example, been found to affect structural cytoskeletal proteins, including intermediate filament proteins and actin (Hofmann et al., 2009; Kaminsky et al., 2009; Snider et al., 2011; Boudreau et al., 2012; Alonso et al., 2015). In addition, sumoylation controls cytoskeletal regulatory proteins, including the actin regulators Rho1 and Rac1 (Castillo-Lluva et al., 2010; Yu et al., 2012), as well as tau and other microtubule-associated proteins (Luo et al., 2014; Abrieu and Liakopoulos, 2019). Beyond these effects of SUMO2 on structural and regulatory cytoskeletal proteins, however, we also observed significant changes at the level of gene expression for genes involved in the epithelial-to-mesenchymal transition (EMT), the extracellular matrix, integrin–cell surface interactions, and genes coding for Wnt-family proteins in the SUMO2 KO cells, which could also contribute to changes in cellular morphology. Thus, it is highly likely that the morphological changes observed in the SUMO2 KO cells are the sum result of the effects of sumoylation at the level of structural proteins, regulatory proteins, and gene expression. It is anticipated that other phenotypic changes that we observed in SUMO1 and SUMO2 KO cells may also be explained through similar, combined effects.

This level of complexity, for example, is also likely to underlie the role of sumoylation in the assembly and function of PML nuclear bodies. In addition to evidence demonstrating that sumoylation directly affects PML protein phase separation (Banani et al., 2016), evidence also suggests that the size and number of these membrane-less organelles are influenced by interactions with chromatin that fluctuate throughout the cell cycle and in response to changes in gene expression, DNA replication, and DNA damage (Corpet et al., 2020). Thus, sumoylation likely affects PML nuclear body size and number through both direct effects on the PML protein and indirect effects on chromatin structure and gene expression. In this regard, it is possible that the failure to rescue PML nuclear body number in our SUMO2 rescue line may be due to irreversible, epigenetic changes in chromatin structure rather than a direct effect on PML nuclear body assembly. However, we cannot rule out possible off-target mutations in the SUMO2 KO cells that may influence PML nuclear body dynamics. Similarly, phenotypes observed in our SUMO1 KO cell line also require verification through analysis of rescue lines and other complementary studies.

The uniqueness of SUMO2 in controlling gene expression

Consistent with evidence that SUMO1 and SUMO2 can exert unique effects on individual regulators of transcription (Holmstrom et al., 2003; Rosendorff et al., 2006; Zheng et al., 2006; Ouyang et al., 2009), our RNA-seq analysis revealed that SUMO1 and SUMO2 paralogues have nonredundant roles in affecting gene expression. These findings are also consistent with ChIP-Seq studies that identi-

fied unique SUMO1 and SUMO2 binding sites across the genome of proliferating human fibroblasts (Neyret-Kahn et al., 2013). Of interest, this study also found that SUMO2 was present at approximately twice the number of binding sites compared with SUMO1, a finding consistent with our identification of nearly twice as many uniquely altered genes in the SUMO2 KO cells as compared with SUMO1 KO cells (at a false discovery rate [FDR] <0.05). We also found that the change in expression of individual genes was, on average, greater in SUMO2 KO cells as compared with SUMO1 KO cells, consistent with reports that SUMO2 can more robustly affect the activity of individual transcription factors (Holmstrom et al., 2003). In addition to differences in the magnitude of change in gene expression, we also made the interesting observation that SUMO1 and SUMO2 can have opposing effects on expression of specific gene sets, including genes involved in type I IFN signaling and histone-coding genes, as discussed below. Taken together, our results reveal that although both SUMO1 and SUMO2 have important and nonredundant roles in regulating gene expression, SUMO2 appears to have a broader and more potent role.

Immune response and histone gene sets affected by SUMO1 and SUMO2

Among intriguing gene sets affected in our SUMO KO cell lines, we found that genes involved in immune response pathways were up-regulated in the SUMO2 KO cells. This finding is consistent with previous studies reporting an increase in expression of inflammatory and anti-viral genes in stimulated myeloid cells deficient in sumoylation (Decque et al., 2016). Moreover, it has also been reported that the specific loss of SUMO2 and SUMO3 expression, but not loss of SUMO1, drives a potent type I IFN response mediated through noncanonical mechanisms (Crowl and Stetson, 2018). These findings are of particular interest in light of ongoing clinical trials with the global sumoylation inhibitor, TAK-981, which is being used to treat solid tumors, and most recently COVID-19 (Sarit Assouline et al., 2019; Presage Biosciences, 2019; Takeda, 2019, 2020). The predicted success of TAK-981 as an anti-cancer and anti-viral therapeutic is based in part on findings that it increases the type I IFN response (Kubota et al., 2008; Schmidt et al., 2019). Thus, understanding the unique effect of SUMO2 in activating immune response genes has the potential to lead to the development of novel and more targeted therapeutics.

We also observed changes in a large number of histone genes in both SUMO1 and SUMO2 KO cell lines. Of particular interest, expression levels increased in SUMO2 KO cells, but decreased in SUMO1 KO cells. Consistent with these findings, it was previously reported that SUMO1 and SUMO2 bind to histone gene promoters and that histone gene expression levels increase upon knockdown of Ubc9 and PIASY (Neyret-Kahn et al., 2013). Our findings reveal that these previously observed effects of sumoylation on histone gene expression may have been due specifically to the loss of SUMO2-modified regulators. Histone gene expression is tightly controlled by the cell cycle, with an approximately 35-fold increase in mRNA levels occurring specifically during S-phase (Duronio and Marzluff, 2017). Our flow cytometry analysis indicated that observed changes in histone gene expression cannot be explained by changes in the cell cycle distribution of SUMO KO cells. Other potential mechanisms could involve differential effects of SUMO1 and SUMO2 on transcriptional activators or repressors, or on factors affecting histone mRNA processing or turnover. The stability of one such factor, FLASH, has previously been reported to be affected specifically by SUMO2/3 modification (Vennemann and Hofmann, 2013), and factors affecting 3'-end processing, including symplekin

and CPSF73, are also regulated by SUMO modification (Duronio and Marzluff, 2017). Also of potential relevance, histone gene expression and mRNA processing are regulated through the assembly of factors at histone gene loci, known as histone locus bodies (Marzluff and Koreski, 2017). Like PML-NBs, the histone locus body has been proposed to assemble in part through liquid–liquid phase separation of associated proteins (Hur et al., 2020). Similar to PML-NBs, it can be predicted that both SUMO1 and SUMO2 play a role in facilitating the recruitment and phase separation of histone locus body–associated proteins and that these functions may be disrupted in the SUMO KO cells.

Molecular features defining SUMO1 and SUMO2 nonredundant functions

Our findings raise the important question of what specific molecular features determine the unique and nonredundant functions of SUMO1 and SUMO2. We anticipate that both association with unique, downstream SIM-containing proteins and differences in the potential to form polymeric chains will be important defining factors. Studies in yeast, which express only a single SUMO, indicate that both SIM binding and an ability to form polymeric chains are critical for function (Bylebyl et al., 2003; Newman et al., 2017). Regarding polymeric chains, however, consensus site lysines in the N-terminal tail of yeast and also zebrafish SUMO are not vital for biological function if lysines at other positions are available (Yuan et al., 2010; Newman et al., 2017). Moreover, K11 of SUMO2 is not required for STUbL-mediated turnover of PML in mammalian cells (Gartner et al., 2018). Thus, whether the consensus lysine at position 11 of human SUMO2/3 is a critical determinant of biological function remains to be fully tested. Our demonstrated ability to rescue SUMO2 KO phenotypes with WT SUMO2 provides the tools to address the functional significance of K11, as well as surface residues of SUMO1 and SUMO2 that confer selective SIM interactions.

Distinct functions for monomeric and polymeric SUMO modification are particularly important in regulating the association of proteins with chromatin. SUMO proteases in yeast and human cells, for example, have a specialized role in facilitating DNA replication initiation, replication stress responses, and other chromatin-associated functions by limiting untimely production of polymeric SUMO chains (Psakhye et al., 2019; Wagner et al., 2019; Kramarz et al., 2020). Thus, it can be speculated that SUMO paralogues with various chain-forming abilities, like SUMO1 and SUMO2, have evolved in higher eukaryotes to further separate the distinct signaling properties of monomeric and polymeric SUMO. In addition to exploring the relevance of differences in chain-forming abilities, further elucidating the nonredundant roles observed for SUMO1 and SUMO2 in regulating gene expression and responses to HU-induced replication stress will also require more deliberate identification and characterization of paralogue-specific substrates. Although a number of studies have identified SUMO2-modfied proteins involved in gene expression and replication stress responses (Seifert et al., 2015; Xiao et al., 2015; Hendriks and Vertegaal, 2016), there have been limited efforts focused on SUMO1 substrate identification. Defining unique roles for SUMO1 and SUMO2 in response to replication stress may be of particular value by providing new insights into mechanisms of HU resistance, which is commonly observed in the cancer clinic (Demuynck et al., 2019).

CONCLUSIONS

In summary, our findings reveal nonredundant roles for SUMO1 and SUMO2 in regulating a diverse range of cellular functions, including control of cell morphology, responses to genotoxic stress, and regulation of gene expression. The findings provide a foundation for further exploring the molecular basis for SUMO1 and SUMO2 function in these processes, as well as the molecular features that distinguish SUMO1 from SUMO2 function. Our findings also highlight a need for more rigorous characterization of SUMO paralogue functions in the context of complex tissues. It is anticipated that further defining the molecular features that distinguish SUMO1 from SUMO2 function and developing a deeper understanding of tissue-specific SUMO paralogue functions will lead to the discovery of novel and more highly targeted SUMO pathway therapeutics.

MATERIALS AND METHODS

Request a protocol through Bio-protocol.

Human cell line and tissue expression analysis

Normalized gene RPKM values from 528 cancer cell lines were downloaded from The CCLE using the 02-JAN-2019 release (Barretina et al., 2012). Student's t tests were used for pairwise comparisons, and p values are listed in the legend of Figure 1. Normal human tissue data were downloaded as normalized gene transcript per million (TPM) values from the GTEx Project Version 8, which is supported by the Common Fund of the Office of the Director of the National Institutes of Health, and by the National Cancer Institute, National Human Genome Research Institute, National Heart, Lung, and Blood Institute, National Institute on Drug Abuse, National Institute of Mental Health, and National Institute of Neurological Disorders and Stroke. The number of samples available for each tissue are labeled in Figure 1. Heatmaps were made in Rstudio, using ggplot2 and the gganatogram package (Wickham, 2016).

CRISPR-Cas9 gene knockout and sequencing validation

Gene-specific knockout of SUMO1 and SUMO2 in U2OS cells using CRISPR-Cas9 was performed according to a previously published protocol (Ran et al., 2013). In brief, single guide RNA (sgRNA) was designed by the CRISPR design tool (http://crispr.mit.edu) as follows: SUMO1 5′-TCCCTCCTCCCTGCGCGAAG-3′; SUMO2 5′-CCTCACCTGTCGTTCACAAT-3′. sgRNA was cloned into the pSpCas9(BB)-2A-GFP vector using Bpil enzyme sites (Thermo Scientific), and the vector was transiently transfected into U2OS cells using X-tremeGENE HP reagent according to the manufacturer's protocol (Roche). Transfected cells expressing green fluorescent protein (GFP) were sorted as single cells into 96-well plates by fluorescence-activated cell sorting (FACS) at The Bloomberg Flow Cytometry and Immunology Core. CRISPR-Cas9–introduced mutations were identified using the Clonetech Guide-it Indel Identification Kit (Clonetech; catalogue number: 631444), following the user's manual. Genomic primer sequences for SUMO1 and SUMO2 are listed in Supplemental Table 1, with Clonetech regions of homology indicated. Ten individual SUMO1 and SUMO2 colonies were sent for Sanger DNA sequencing at the Johns Hopkins University Genetic Resources Core Facility. Aligned sequence reads surrounding the mutation sites are in Supplemental Figures 2 and 3. U2OS WT, SUMO1 KO, and SUMO2 KO cells were confirmed free of mycoplasma contamination using the Promokline PCR Mycoplasma Test Kit I/C (catalogue number: PK-CA91-1024) following the vendor protocol.

Cell lines and cell culture conditions

U2OS WT, SUMO1 KO, SUMO2 KO, SUMO2KO+SUMO2, and SUMO2KO+SUMO1 cells were grown at 37°C, 5% CO_2 in Life Technologies DMEM (catalogue number: 11965-092) supplemented with 10% fetal bovine serum (FBS) (Atlanta Biologics; catalogue number: S11550).

Generation of stable rescue cell lines

Plasmids encoding precursor SUMO1 or SUMO2 were acquired from TWIST Bioscience on a pTWIST CMV Puro vector (Supplemental Figure 6). SUMO2 KO cells (2×10^5) grown overnight were transfected with 1 µg of pTWIST plasmids using Lipofectamine 2000 (Invitrogen; catalogue number 1881535), following standard protocols. Fresh Life Technologies DMEM with 10% FBS was supplied after 6 h of incubation. Puromycin (Sigma; catalogue number: P8833) selection was performed 48 h posttransfection at a final concentration of 2 ng/ml for 4–5 d. Stable rescue cell lines were obtained by single-cell cloning and maintained in 1 ng/ml puromycin-containing DMEM for a month and then grown in standard conditions, as above. SUMO paralogue expression levels in the rescue cell lines were validated by immunofluorescence microscopy and immunoblotting with corresponding antibodies, per Supplemental Table 2.

Immunoblotting and semiquantification of SUMO levels

Cells were lysed with 2× Laemmli buffer (4% SDS, 20% glycerol, 125 mM Tris-Cl, pH 6.8, 10% 2-mercaptoethanol, 0.02% bromophenol blue) and denatured at 95°C for 5 min. Whole cell lysate was loaded onto 10% SDS–polyacrylamide gels and transferred onto polyvinylidene difluoride (PVDF) membrane. Membranes were briefly washed with 1× Tris-buffered saline (TBS) and blocked in 5% milk (in TBS) followed by incubation with anti-SUMO primary antibodies (SUMO1: [1:1000]; SUMO2: [1:800]; tubulin: [1:10,000]) overnight at 4°C, washed 3 × 10 min with TBS with 0.5% Tween 20 (TBS-T), and incubated with horseradish peroxidase (HRP)-conjugated secondary antibodies ([1:10,000]) in 5% milk for 1 h at room temperature, followed by washing for 3 × 10 min with 1× TBS-T. Bound antibodies were visualized by autoradiography following incubation of membranes with Amersham ECL prime Western blotting detection reagent (catalogue number 45-002-401). Immunoblot signal intensities were quantified using FIJI image processing software (Schindelin et al., 2012) and normalized to corresponding tubulin loading controls.

Immunofluorescence microscopy and quantitative cell morphology analysis

Cells (2.5×10^5 cells/coverslip) were seeded in a six-well dish and grown overnight, washed with phosphate-buffered saline (PBS), and fixed in 4% paraformaldehyde in PBS for 20 min, followed by permeabilization in 0.05% Triton X-100 in PBS for 20 min. Cells were then incubated with anti-SUMO and anti-tubulin primary antibodies (Supplemental Table 2) for 1 h, washed in PBS with 0.5% Tween (PBS-T), and incubated with Alexa fluorescent secondary antibodies (Supplemental Table 2) for 40 min. Coverslips were then mounted using Fluoroshield Mounting Medium with 4′,6-diamidino-2-phenylindole (DAPI; Abcam; catalogue number: ab104139). Microscopy images were taken using an upright Zeiss Observer Z1 fluorescence microscope with an Apotome V_H optical section grid. Representative images showing SUMO protein levels and morphology of each cell line were taken using a 40× objective. Quantitative analysis of cellular morphology, including measurements of cellular aspect ratio, area, and circularity, was performed using built-in measurement functions of FIJI software (Schindelin et al., 2012). For each cell line, at least 800 cells from three independent experiments were measured. The Kruskal–Wallis nonparametric test was used for statistical comparison and calculation of p values.

Flow cytometry

Cells (4.5×10^6) were fixed in ice cold 70% EtOH and stained with propidium iodide in triplicate, following a standard protocol (Darzynkiewicz et al., 2001). Cells were analyzed using a BD LSRII flow cytometer. BD FACSDiva acquisition software was used to acquire 5.0×10^4 single events per sample, and G0 cells were centered on 100. FloJo version 10.6.1 was used for analysis. Statistics were calculated using an analysis of variance (ANOVA), and p values are labeled on the final plots, made using ggplot in RStudio (Wickham, 2016).

Quantitative nuclear body imaging and analysis

Cells were seeded at 2.5×10^5 cells/coverslip in a six-well dish and grown overnight. Cells were rinsed with PBS, fixed in 3.5% paraformaldehyde in PBS for 7 min, and permeabilized in PBS-T for 20 min. Cells were then incubated for 1 h with primary antibodies (Supplemental Table 2), washed with PBS-T, and incubated for 35 min with fluorescently labeled secondary antibodies (Supplemental Table 2). Microscopy images were taken using an upright Zeiss Observer Z1 fluorescence microscope with an Apotome V_H optical section grid. Nonsaturated 16-bit gray images were exported from the AxioVision Release 4.8 software and opened in FIJI (Schindelin et al., 2012). Nuclei (DAPI) and foci (dsRED and/or GFP) signal thresholds were set using the RenyiEntropy algorithm, and the Speckle Inspector function of the Biovoxxel plug-in (Kapur et al., 1985; Brocher, 2014) was used to quantitate the number of foci per nucleus, foci signal intensity, and foci perimeters. A nonparametric Wilcoxin test was used to calculate p values in R, and graphs were generated using ggplot2.

Cellular viability analysis

Cells (2×10^3 per well) were plated into 96-well plates in 100 µl of media and grown overnight. Each cell line was seeded in triplicate for each dose of the drug treatment. Treatments were performed with the concentrations and times indicated on each figure, using -azetidine-2-carboxylic acid (Sigma A0760-50MG), EerI (EMD Millipore 324521-25MG), or hydroxyurea (Amresco; 1B1368-25G). After drug treatment, each well was washed once with PBS, and then 100 µl of DMEM (without phenol red; Life Technologies; catalogue number 21063-029) containing 10% FBS and 10 µl of 12 mM MTT (3-[4,5-dimethylthiazol-2-yl]-2,5-diphenyl tetrazolium bromide; Molecular Probes V-13154) were added to each well, including a negative control of 10 µl of the MTT solution added to 100 µl of medium alone. After 4 h of incubation at 37°C with 5% CO_2, 80 µl of the media was removed from each well, and 50 µl of dimethyl sulfoxide (DMSO) was added to solubilize the metabolized insoluble formazan product. After incubation at 37°C for 10 min, 96-well plates were analyzed using a fluorescence plate reader (BioTek Synergy HT) at an absorbance of 540 nm. For the analysis, the negative control signal was deducted from all wells before relative cell viability was calculated for each treated group as a percentage of the untreated group for each cell line.

Transcriptome analysis and data visualization

Total RNA isolation, QC, and library preparation from three biological replicates of each authenticated and validated U2OS parental, SUMO1 KO, and SUMO2 KO cell line was performed by Novogene. Transcriptomic data from the three cell lines and biological replicates were generated using an Illumina HiSeq 4000 sequencer. Paired-end reads were obtained with a read depth of more than 60 million reads per sample. The reads were cleaned and mapped to the reference genome using STAR, HTseq, Cufflink, and Tophat programs. This resulted in a total of 48,162 Ensembl reads. Of those, 23,758 were mapped to Entrez gene IDs and used in downstream analysis. Genes were filtered to keep those that had approximately

10 or more read counts in at least all three replicates of one cell type, which resulted in a total of 14,999 genes for downstream analysis (Law *et al.*, 2016). Reads were evenly distributed throughout the genome, and both a multidimensional scaling (MDS) plot and calculated Pearson correlations among replicates demonstrated highly consistent read counts with minimal variance between biological replicates (Supplemental Figure 7). The sequencing data and processed files were deposited in the GEO database under accession code GSE163884.

The Karyoplotter package was used to visualize mapped differentially expressed genes (DEGs) along individual human chromosomes in RStudio (Gel and Serra, 2017). Pathway enrichment analysis using GSEA (version 4.0.3) from the Broad Institute and visualization of the data using Cytoscape and EnrichmentMap were performed following published protocols (Subramanian *et al.*, 2005; Reimand *et al.*, 2019). The GSEA algorithm calculates GO enrichments from a list of global gene expression values, not just those that meet a specific threshold criterion. Specifically, GSEA used the expression values of the same 14,999 genes from the SUMO1 and SUMO2 KO cells to generate two ranked lists of genes (one for each KO cell as compared with WT), which were then tested for gene set enrichments. For the analysis, .gct data of FPKM values for all three replicates for all three samples and a phenotypes .cls file were loaded into GSEA. One thousand permutations were used and collapsed to match the Human NCBI Entrez GENE ID MSigDBv.7.1.chip platform; otherwise default settings were used. Results were compiled and analyzed in RStudio using GeneEnricher. Cytoscape (version 3.8.0 using Java 11.0.6) was used to visualize IFN and collagen gene sets.

qRT-PCR for DEG validation and rescue experiments
Cells were seeded at 5.0×10^5 cells/well in 3.5 mm dishes and grown overnight. Total RNA was extracted using the Sigma GenElute Mammalian MiniPrep kit (Sigma; catalogue number RTN70) following the vendor's protocol. Extracted RNA was analyzed by nanodrop for concentration and purity. cDNA was generated using the New England BioLab ProtoScript First Strand cDNA Synthesis Kit (catalogue number E6300S) with 250 ng of RNA and following the vendor's protocol. Poly-d(T)$_{23}$ VN primers were used to generate cDNA for all genes except for histone genes, for which random-hexamer primers were used as histone mRNAs do not contain polyA tails. The quantitative PCR (qPCR) was performed using Applied Biosystems PowerUp SYBR green master mix (catalogue number A25742) following the vendor's recommended protocol. qPCR runs were performed using Applied Biosystems Quant Studio with Quant Studio v1.3.1 software. Gene expression was calculated from three biological replicates, each run in triplicate, using the Ct method and GAPDH as a validated housekeeping gene. A list of primer sequences can be found in Supplemental Table 1.

REFERENCES
Abrieu A, Liakopoulos D (2019). How does SUMO participate in spindle organization? Cells 8, 801.

Adorisio S, Fierabracci A, Muscari I, Liberati AM, Ayroldi E, Migliorati G, Thuy TT, Riccardi C, Delfino DV (2017). SUMO proteins: guardians of immune system. J Autoimmun 84, 21–28.

Alkuraya FS, Saadi I, Lund JJ, Turbe-Doan A, Morton CC, Maas RL (2006). SUMO1 haploinsufficiency leads to cleft lip and palate. Science 313, 1751.

Alonso A, Greenlee M, Matts J, Kline J, Davis KJ, Miller RK (2015). Emerging roles of sumoylation in the regulation of actin, microtubules, intermediate filaments, and septins. Cytoskeleton (Hoboken) 72, 305–339.

Augustine RC, Vierstra RD (2018). SUMOylation: re-wiring the plant nucleus during stress and development. Curr Opin Plant Biol 45, 143–154.

Ayaydin F, Dasso M (2004). Distinct in vivo dynamics of vertebrate SUMO paralogues. Mol Biol Cell 15, 5208–5218.

Baczyk D, Audette MC, Coyaud E, Raught B, Kingdom JC (2018). Spatiotemporal distribution of small ubiquitin-like modifiers during human placental development and in response to oxidative and inflammatory stress. J Physiol 596, 1587–1600.

Banani SF, Rice AM, Peeples WB, Lin Y, Jain S, Parker R, Rosen MK (2016). Compositional control of phase-separated cellular bodies. Cell 166, 651–663.

Barretina J, Caponigro G, Stransky N, Venkatesan K, Margolin AA, Kim S, Wilson CJ, Lehar J, Kryukov GV, Sonkin D, et al. (2012). The Cancer Cell Line Encyclopedia enables predictive modelling of anticancer drug sensitivity. Nature 483, 603–607.

Becker J, Barysch SV, Karaca S, Dittner C, Hsiao HH, Berriel Diaz M, Herzig S, Urlaub H, Melchior F (2013). Detecting endogenous SUMO targets in mammalian cells and tissues. Nat Struct Mol Biol 20, 525–531.

Boudreau E, Labib S, Bertrand AT, Decostre V, Bolongo PM, Sylvius N, Bonne G, Tesson F (2012). Lamin a/c mutants disturb sumo1 localization and sumoylation in vitro and in vivo. PLoS One 7, e45918.

Brem GJ, Mylonas I, Bruning A (2013). Eeyarestatin causes cervical cancer cell sensitization to bortezomib treatment by augmenting ER stress and CHOP expression. Gynecol Oncol 128, 383–390.

Brocher J (2014). Qualitative and quantitative evaluation of two new histogram limiting binarization algorithms. Intl J Image Processing 8, 30–48.

Bylebyl GR, Belichenko I, Johnson ES (2003). The SUMO isopeptidase Ulp2 prevents accumulation of SUMO chains in yeast. J Biol Chem 278, 44113–44120.

Cappadocia L, Lima CD (2018). Ubiquitin-like protein conjugation: structures, chemistry, and mechanism. Chem Rev 118, 889–918.

Castillo-Lluva S, Tatham MH, Jones RC, Jaffray EG, Edmondson RD, Hay RT, Malliri A (2010). SUMOylation of the GTPase Rac1 is required for optimal cell migration. Nat Cell Biol 12, 1078–1085.

Chang CC, Naik MT, Huang YS, Jeng JC, Liao PH, Kuo HY, Ho CC, Hsieh YL, Lin CH, Huang NJ, et al. (2011). Structural and functional roles of Daxx SIM phosphorylation in SUMO paralog-selective binding and apoptosis modulation. Mol Cell 42, 62–74.

Chang HM, Yeh ETH (2020). SUMO: from bench to bedside. Physiol Rev 100, 1599–1619.

Chang PC, Cheng CY, Campbell M, Yang YC, Hsu HW, Chang TY, Chu CH, Lee YW, Hung CL, Lai SM, et al. (2013). The chromatin modification by SUMO-2/3 but not SUMO-1 prevents the epigenetic activation of key immune-related genes during Kaposi's sarcoma associated herpesvirus reactivation. BMC Genomics 14, 824.

Citro S, Chiocca S (2013). Sumo paralogs: redundancy and divergencies. Front Biosci 5, 544–553.

Corpet A, Kleijwegt C, Roubille S, Juillard F, Jacquet K, Texier P, Lomonte P (2020). PML nuclear bodies and chromatin dynamics: catch me if you can! Nucleic Acids Res 48, 11890–11912.

Crowl JT, Stetson DB (2018). SUMO2 and SUMO3 redundantly prevent a noncanonical type I interferon response. Proc Natl Acad Sci USA 115, 6798–6803.

Cubenas-Potts C, Goeres JD, Matunis MJ (2013). SENP1 and SENP2 affect spatial and temporal control of sumoylation in mitosis. Mol Biol Cell 24, 3483–3495.

Cubenas-Potts C, Matunis MJ (2013). SUMO: a multifaceted modifier of chromatin structure and function. Dev Cell 24, 1–12.

Cubenas-Potts C, Srikumar T, Lee C, Osula O, Subramonian D, Zhang XD, Cotter RJ, Raught B, Matunis MJ (2015). Identification of SUMO-2/3-modified proteins associated with mitotic chromosomes. Proteomics 15, 763–772.

Darzynkiewicz Z, Juan G, Bedner E (2001). Determining cell cycle stages by flow cytometry. Curr Protoc Cell Biol Chapter 8, Unit 8.4.

Dasso M (2008). Emerging roles of the SUMO pathway in mitosis. Cell Div 3, 5.

Decque A, Joffre O, Magalhaes JG, Cossec JC, Blecher-Gonen R, Lapaquette P, Silvin A, Manel N, Joubert PE, Seeler JS, *et al.* (2016). Sumoylation coordinates the repression of inflammatory and anti-viral gene-expression programs during innate sensing. Nat Immunol 17, 140–149.

Demuynck T, Verhoef G, Delforge M, Vandenberghe P, Devos T (2019). Polycythemia vera and hydroxyurea resistance/intolerance: a monocentric retrospective analysis. Ann Hematol 98, 1421–1426.

Duronio RJ, Marzluff WF (2017). Coordinating cell cycle-regulated histone gene expression through assembly and function of the histone locus body. RNA Biol 14, 726–738.

Eifler K, Vertegaal ACO (2015). SUMOylation-mediated regulation of cell cycle progression and cancer. Trends Biochem Sci 40, 779–793.

Enserink JM (2015). Sumo and the cellular stress response. Cell Div 10, 4.

Evdokimov E, Sharma P, Lockett SJ, Lualdi M, Kuehn MR (2008). Loss of SUMO1 in mice affects RanGAP1 localization and formation of PML nuclear bodies, but is not lethal as it can be compensated by SUMO2 or SUMO3. J Cell Sci 121, 4106–4113.

Gartner A, Wagner K, Holper S, Kunz K, Rodriguez MS, Muller S (2018). Acetylation of SUMO2 at lysine 11 favors the formation of non-canonical SUMO chains. EMBO Rep 19, 46117.

Gel B, Serra E (2017). karyoploteR: an R/Bioconductor package to plot customizable genomes displaying arbitrary data. Bioinformatics 33, 3088–3090.

Ghisletti S, Huang W, Ogawa S, Pascual G, Lin ME, Willson TM, Rosenfeld MG, Glass CK (2007). Parallel SUMOylation-dependent pathways mediate gene- and signal-specific transrepression by LXRs and PPARgamma. Mol Cell 25, 57–70.

Gill G (2005). Something about SUMO inhibits transcription. Curr Opin Genet Dev 15, 536–541.

Gong L, Li DW (2010). SUMOylation in ocular development and pathology. Curr Mol Med 10, 794–801.

Gry M, Rimini R, Stromberg S, Asplund A, Ponten F, Uhlen M, Nilsson P (2009). Correlations between RNA and protein expression profiles in 23 human cell lines. BMC Genomics 10, 365.

Hasegawa Y, Yoshida D, Nakamura Y, Sakakibara S (2014). Spatiotemporal distribution of SUMOylation components during mouse brain development. J Comp Neurol 522, 3020–3036.

Hay RT (2013). Decoding the SUMO signal. Biochem Soc Trans 41, 463–473.

Hecker CM, Rabiller M, Haglund K, Bayer P, Dikic I (2006). Specification of SUMO1- and SUMO2-interacting motifs. J Biol Chem 281, 16117–16127.

Hendriks IA, Vertegaal AC (2016). A comprehensive compilation of SUMO proteomics. Nat Rev Mol Cell Biol 17, 581–595.

Hickey CM, Wilson NR, Hochstrasser M (2012). Function and regulation of SUMO proteases. Nat Rev Mol Cell Biol 13, 755–766.

Hofmann WA, Arduini A, Nicol SM, Camacho CJ, Lessard JL, Fuller-Pace FV, de Lanerolle P (2009). SUMOylation of nuclear actin. J Cell Biol 186, 193–200.

Holmstrom S, Van Antwerp ME, Iniguez-Lluhi JA (2003). Direct and distinguishable inhibitory roles for SUMO isoforms in the control of transcriptional synergy. Proc Natl Acad Sci USA 100, 15758–15763.

Hur W, Kemp JP Jr, Tarzia M, Deneke VE, Marzluff WF, Duronio RJ, Di Talia S (2020). CDK-regulated phase separation seeded by histone genes ensures precise growth and function of histone locus bodies. Dev Cell 54, 379–394.e376.

Jansen NS, Vertegaal ACO (2021). A chain of events: regulating target proteins by SUMO polymers. Trends Biochem Sci 46, 113–123.

Joseph J, Tan SH, Karpova TS, McNally JG, Dasso M (2002). SUMO-1 targets RanGAP1 to kinetochores and mitotic spindles. J Cell Biol 156, 595–602.

Kaminsky R, Denison C, Bening-Abu-Shach U, Chisholm AD, Gygi SP, Broday L (2009). SUMO regulates the assembly and function of a cytoplasmic intermediate filament protein in C. elegans. Dev Cell 17, 724–735.

Kapur JN, Sahoo PK, Wong AKC (1985). A new method for gray-level picture thresholding using the entropy of the histogram. Comput Vision Graph 29, 273–285.

Karhausen J, Bernstock JD, Johnson KR, Sheng H, Ma Q, Shen Y, Yang W, Hallenbeck JM, Paschen W (2018). Ubc9 overexpression and SUMO1 deficiency blunt inflammation after intestinal ischemia/reperfusion. Lab Invest 98, 799–813.

Kramarz K, Schirmeisen K, Boucherit V, Ait Saada A, Lovo C, Palancade B, Freudenreich C, Lambert SAE (2020). The nuclear pore primes recombination-dependent DNA synthesis at arrested forks by promoting SUMO removal. Nat Commun 11, 5643.

Kubota T, Matsuoka M, Chang TH, Tailor P, Sasaki T, Tashiro M, Kato A, Ozato K (2008). Virus infection triggers SUMOylation of IRF3 and IRF7, leading to the negative regulation of type I interferon gene expression. J Biol Chem 283, 25660–25670.

Kunz K, Piller T, Muller S (2018). SUMO-specific proteases and isopeptidases of the SENP family at a glance. J Cell Sci 131, jcs211904.

Lallemand-Breitenbach V, de The H (2010). PML nuclear bodies. Cold Spring Harb Perspect Biol 2, a000661.

Lallemand-Breitenbach V, de The H (2018). PML nuclear bodies: from architecture to function. Curr Opin Cell Biol 52, 154–161.

Law CW, Alhamdoosh M, Su S, Dong X, Tian L, Smyth GK, Ritchie ME (2016). RNA-seq analysis is easy as 1-2-3 with limma, Glimma and edgeR. F1000Res 5. ISCB Comm J-1408.

Lee CC, Li B, Yu H, Matunis MJ (2018). Sumoylation promotes optimal APC/C activation and timely anaphase. eLife 7, e29539.

Liang YC, Lee CC, Yao YL, Lai CC, Schmitz ML, Yang WM (2016). SUMO5, a novel poly-SUMO isoform, regulates PML nuclear bodies. Sci Rep 6, 26509.

Luo HB, Xia YY, Shu XJ, Liu ZC, Feng Y, Liu XH, Yu G, Yin G, Xiong YS, Zeng K, *et al.* (2014). SUMOylation at K340 inhibits tau degradation through deregulating its phosphorylation and ubiquitination. Proc Natl Acad Sci USA 111, 16586–16591.

Marzluff WF, Koreski KP (2017). Birth and death of histone mRNAs. Trends Genet 33, 745–759.

McKibbin C, Mares A, Piacenti M, Williams H, Roboti P, Puumalainen M, Callan AC, Lesiak-Mieczkowska K, Linder S, Harant H, *et al.* (2012). Inhibition of protein translocation at the endoplasmic reticulum promotes activation of the unfolded protein response. Biochem J 442, 639–648.

Meulmeester E, Kunze M, Hsiao HH, Urlaub H, Melchior F (2008). Mechanism and consequences for paralog-specific sumoylation of ubiquitin-specific protease 25. Mol Cell 30, 610–619.

Mikkonen L, Hirvonen J, Janne OA (2013). SUMO-1 regulates body weight and adipogenesis via PPARgamma in male and female mice. Endocrinology 154, 698–708.

Mukhopadhyay D, Arnaoutov A, Dasso M (2010). The SUMO protease SENP6 is essential for inner kinetochore assembly. J Cell Biol 188, 681–692.

Namanja AT, Li YJ, Su Y, Wong S, Lu J, Colson LT, Wu C, Li SS, Chen Y (2012). Insights into high affinity small ubiquitin-like modifier (SUMO) recognition by SUMO-interacting motifs (SIMs) revealed by a combination of NMR and peptide array analysis. J Biol Chem 287, 3231–3240.

Newman HA, Meluh PB, Lu J, Vidal J, Carson C, Lagesse E, Gray JJ, Boeke JD, Matunis MJ (2017). A high throughput mutagenic analysis of yeast sumo structure and function. PLoS Genet 13, e1006612.

Neyret-Kahn H, Benhamed M, Ye T, Le Gras S, Cossec JC, Lapaquette P, Bischof O, Ouspenskaia M, Dasso M, Seeler J, *et al.* (2013). Sumoylation at chromatin governs coordinated repression of a transcriptional program essential for cell growth and proliferation. Genome Res 23, 1563–1579.

Ouyang J, Shi Y, Valin A, Xuan Y, Gill G (2009). Direct binding of CoREST1 to SUMO-2/3 contributes to gene-specific repression by the LSD1/CoREST1/HDAC complex. Mol Cell 34, 145–154.

Presage Biosciences (2019). Intratumoral microdosing of TAK-981 in head and neck cancer.

Psakhye I, Castellucci F, Branzei D (2019). SUMO-chain-regulated proteasomal degradation timing exemplified in DNA replication initiation. Mol Cell 76, 632–645.e6.

Ran FA, Hsu PD, Wright J, Agarwala V, Scott DA, Zhang F (2013). Genome engineering using the CRISPR-Cas9 system. Nat Protoc 8, 2281–2308.

Reimand J, Isserlin R, Voisin V, Kucera M, Tannus-Lopes C, Rostamianfar A, Wadi L, Meyer M, Wong J, Xu C, *et al.* (2019). Pathway enrichment analysis and visualization of omics data using g:Profiler, GSEA, Cytoscape and EnrichmentMap. Nat Protoc 14, 482–517.

Rosendorff A, Sakakibara S, Lu S, Kieff E, Xuan Y, DiBacco A, Shi Y, Shi Y, Gill G (2006). NXP-2 association with SUMO-2 depends on lysines required for transcriptional repression. Proc Natl Acad Sci USA 103, 5308–5313.

Rosonina E, Akhter A, Dou Y, Babu J, Sri Theivakadadcham VS (2017). Regulation of transcription factors by sumoylation. Transcription 8, 220–231.

Saitoh H, Hinchey J (2000). Functional heterogeneity of small ubiquitin-related protein modifiers SUMO-1 versus SUMO-2/3. J Biol Chem 275, 6252–6258.

Sarit Assouline AM, Caimi PF, Wang B, Patel C, Kim M-S, Huszar D, Berger AJ, Friedlander S, Gomez-Pinillos A, Proscurshim I (2019). A phase 1b/2 study of TAK-981, a first-in-class sumoylation inhibitor, in combination with rituximab in patients with relapsed/refractory (r/r) CD20-positive non-Hodgkin lymphoma (NHL). Blood 134 (Suppl 1), 1593.

Schindelin J, Arganda-Carreras I, Frise E, Kaynig V, Longair M, Pietzsch T, Preibisch S, Rueden C, Saalfeld S, Schmid B, *et al.* (2012). Fiji: an open-source platform for biological-image analysis. Nat Methods 9, 676–682.

Schmidt N, Domingues P, Golebiowski F, Patzina C, Tatham MH, Hay RT, Hale BG (2019). An influenza virus-triggered SUMO switch orchestrates co-opted endogenous retroviruses to stimulate host antiviral immunity. Proc Natl Acad Sci USA 116, 17399–17408.

Seeler JS, Dejean A (2001). SUMO: of branched proteins and nuclear bodies. Oncogene 20, 7243–7249.

Seifert A, Schofield P, Barton GJ, Hay RT (2015). Proteotoxic stress reprograms the chromatin landscape of SUMO modification. Sci Signal 8, rs7.

Singh A, Xu YJ (2016). The cell killing mechanisms of hydroxyurea. Genes (Basel) 7, 99.

Snider NT, Weerasinghe SV, Iniguez-Lluhi JA, Herrmann H, Omary MB (2011). Keratin hypersumoylation alters filament dynamics and is a marker for human liver disease and keratin mutation. J Biol Chem 286, 2273–2284.

Sriramachandran AM, Dohmen RJ (2014). SUMO-targeted ubiquitin ligases. Biochim Biophys Acta 1843, 75–85.

Subramanian A, Tamayo P, Mootha VK, Mukherjee S, Ebert BL, Gillette MA, Paulovich A, Pomeroy SL, Golub TR, Lander ES, Mesirov JP (2005). Gene set enrichment analysis: a knowledge-based approach for interpreting genome-wide expression profiles. Proc Natl Acad Sci USA 102, 15545–15550.

Takeda (2019). A study of TAK-981 in combination with rituximab in participants with relapsed/refractory (r/r) CD20-positive (CD20+) non-Hodgkin lymphoma (NHL).

Takeda (2020). A safety and efficacy study of TAK-981 plus pembrolizumab in participants with select advanced or metastatic solid tumors.

Tatham MH, Jaffray E, Vaughan OA, Desterro JM, Botting CH, Naismith JH, Hay RT (2001). Polymeric chains of SUMO-2 and SUMO-3 are conjugated to protein substrates by SAE1/SAE2 and Ubc9. J Biol Chem 276, 35368–35374.

Urena E, Pirone L, Chafino S, Perez C, Sutherland JD, Lang V, Rodriguez MS, Lopitz-Otsoa F, Blanco FJ, Barrio R, Martin D (2016). Evolution of SUMO function and chain formation in insects. Mol Biol Evol 33, 568–584.

van Meerloo J, Kaspers GJ, Cloos J (2011). Cell sensitivity assays: the MTT assay. Methods Mol Biol 731, 237–245.

Vennemann A, Hofmann TG (2013). SUMO regulates proteasome-dependent degradation of FLASH/Casp8AP2. Cell Cycle 12, 1914–1921.

Wagner K, Kunz K, Piller T, Tascher G, Holper S, Stehmeier P, Keiten-Schmitz J, Schick M, Keller U, Muller S (2019). The SUMO isopeptidase SENP6 functions as a rheostat of chromatin residency in genome maintenance and chromosome dynamics. Cell Rep 29, 480–494.e485.

Wang CY, She JX (2008). SUMO4 and its role in type 1 diabetes pathogenesis. Diabetes Metab Res Rev 24, 93–102.

Wang L, Wansleeben C, Zhao S, Miao P, Paschen W, Yang W (2014). SUMO2 is essential while SUMO3 is dispensable for mouse embryonic development. EMBO Rep 15, 878–885.

Wang Q, Li L, Ye Y (2008). Inhibition of p97-dependent protein degradation by Eeyarestatin I. J Biol Chem 283, 7445–7454.

Wang Q, Shinkre BA, Lee JG, Weniger MA, Liu Y, Chen W, Wiestner A, Trenkle WC, Ye Y (2010). The ERAD inhibitor eeyarestatin I is a bifunctional compound with a membrane-binding domain and a p97/VCP inhibitory group. PLoS One 5, e15479.

Wasik U, Filipek A (2014). Non-nuclear function of sumoylated proteins. Biochim Biophys Acta 1843, 2878–2885.

Wickham H (2016). ggplot2: Elegant Graphics for Data Analysis, New York: Springer-Verlag.

Xiao Z, Chang JG, Hendriks IA, Sigurethsson JO, Olsen JV, Vertegaal AC (2015). System-wide analysis of SUMOylation dynamics in response to replication stress reveals novel small ubiquitin-like modified target proteins and acceptor lysines relevant for genome stability. Mol Cell Proteomics 14, 1419–1434.

Yu J, Zhang D, Liu J, Li J, Yu Y, Wu XR, Huang C (2012). RhoGDI SUMOylation at Lys-138 increases its binding activity to Rho GTPase and its inhibiting cancer cell motility. J Biol Chem 287, 13752–13760.

Yuan H, Zhou J, Deng M, Liu X, Le Bras M, de The H, Chen SJ, Chen Z, Liu TX, Zhu J (2010). Small ubiquitin-related modifier paralogs are indispensable but functionally redundant during early development of zebrafish. Cell Res 20, 185–196.

Yukita A, Michiue T, Danno H, Asashima M (2007). XSUMO-1 is required for normal mesoderm induction and axis elongation during early Xenopus development. Dev Dyn 236, 2757–2766.

Zagari A, Nemethy G, Scheraga HA (1990). The effect of the L-azetidine-2-carboxylic acid residue on protein conformation. I. Conformations of the residue and of dipeptides. Biopolymers 30, 951–959.

Zhang FP, Mikkonen L, Toppari J, Palvimo JJ, Thesleff I, Janne OA (2008a). Sumo-1 function is dispensable in normal mouse development. Mol Cell Biol 28, 5381–5390.

Zhang XD, Goeres J, Zhang H, Yen TJ, Porter AC, Matunis MJ (2008b). SUMO-2/3 modification and binding regulate the association of CENP-E with kinetochores and progression through mitosis. Mol Cell 29, 729–741.

Zhao X (2018). SUMO-mediated regulation of nuclear functions and signaling processes. Mol Cell 71, 409–418.

Zheng Z, Cai C, Omwancha J, Chen SY, Baslan T, Shemshedini L (2006). SUMO-3 enhances androgen receptor transcriptional activity through a sumoylation-independent mechanism in prostate cancer cells. J Biol Chem 281, 4002–4012.

Zhu J, Zhu S, Guzzo CM, Ellis NA, Sung KS, Choi CY, Matunis MJ (2008). Small ubiquitin-related modifier (SUMO) binding determines substrate recognition and paralog-selective SUMO modification. J Biol Chem 283, 29405–29415.